Research Square

Preprints are preliminary reports that have not undergone peer review.
They should not be considered conclusive, used to inform clinical practice,
or referenced by the media as validated information.

Ethylene signal-driven plant-multitrophic association boosts crop performance

Peng Yu

pengyu.yu@tum.de

Technicial University of Munich https://orcid.org/0000-0003-1670-8428

Marcel Baer

Crop Functional Genomics, Institute of Crop Science and Resource Conservation (INRES), University of Bonn, 53113 Bonn, Germany

Yanting Zhong

China Agricultural University

Baogang Yu

Plant Genetics, TUM School of Life Sciences, Technical University of Munich

Tian Tian

Plant Genetics, TUM School of Life Sciences, Technical University of Munich

Xiaoming He

Crop Functional Genomics, Institute of Crop Science and Resource Conservation (INRES), University of Bonn, 53113 Bonn, Germany

Xiaofang Huang

Plant Genetics, TUM School of Life Sciences, Technical University of Munich, Freising 85354, Germany https://orcid.org/0009-0005-2260-7238

Elena Gallina

Institute for Plant Sciences, Cologne Biocenter, Cluster of Excellence on Plant Sciences, University of Cologne

Isabelle Metzen

Institute for Plant Sciences, Cologne Biocenter, Cluster of Excellence on Plant Sciences, University of Cologne

Rentao Song

China Agricultural University https://orcid.org/0000-0003-1810-9875

Caroline Gutjahr

Max-Planck-Institut für molekulare Pflanzenphysiologie, Potsdam-Golm https://orcid.org/0000-0001-6163-745X

Zhen Su

China Agricultural University

Yudelsy Tandron Moya

Molecular Plant Nutrition, Leibniz Institute of Plant Genetics and Crop Plant Research (IPK) https://orcid.org/0000-0002-7511-0779

Nicolaus von Wiren
Leibniz Institute of Plant Genetics and Crop Plant Research (IPK) https://orcid.org/0000-0002-4966-425X

Siji Wang
State Key Laboratory of Nutrient Use and Management, Frontiers Science Center for Molecular Design Breeding, College of Resources and Environmental Sciences, China Agricultural University

Zheng Zhao
State Key Laboratory of Nutrient Use and Management, Frontiers Science Center for Molecular Design Breeding, College of Resources and Environmental Sciences, China Agricultural University

Lin Zhang
China Agricultural University https://orcid.org/0000-0002-1663-5620

Lixing Yuan
China Agricultural University https://orcid.org/0000-0003-0233-6184

Yunlu Shi
Center for Crop Functional Genomics and Molecular Breeding, China Agricultural University

Mareike Baer
Institute of Nutritional and Food Sciences, Food Microbiology and Hygiene, University of Bonn

Weiwei Qi
Shanghai University

Marcel Bucher
Universitaet zu Koeln https://orcid.org/0000-0003-1680-9413

Chunjian Li
China Agricultural University

Xuexian Li
China Agricultural University https://orcid.org/0000-0002-0863-9250

Frank Hochholdinger
University of Bonn

Article

Keywords: Arbuscular mycorrhizal fungi, Massilia, Ethylene response factor, Flavonoids, Lateral root, Maize, Pericycle

Posted Date: April 30th, 2026

DOI: https://doi.org/10.21203/rs.3.rs-9344086/v1

License: This work is licensed under a Creative Commons Attribution 4.0 International License.
Read Full License

Additional Declarations: There is **NO** Competing Interest.

Ethylene signal-driven plant-multitrophic association boosts crop performance

Marcel Baer[1,2,3,#], Yanting Zhong[4,#], Baogang Yu[2,#], Tian Tian[2], Xiaoming He[1,3], Xiaofang Huang[2], Elena Gallina[5], Isabelle Elisabeth Metzen[5], Rentao Song[6,15], Caroline Gutjahr[7,13], Zhen Su[8], Yudelsy A.T. Moya[9], Nicolaus von Wirén[9], Siji Wang[10], Zheng Zhao[10], Lin Zhang[10], Lixing Yuan[10], Yunlu Shi[11], Mareike Baer[12], Weiwei Qi[14], Marcel Bucher[5], Chunjian Li[4], Xuexian Li[4,*], Frank Hochholdinger[3,**], Peng Yu[1,2,***]

[1] Emmy Noether Group Root Functional Biology, Institute of Crop Science and Resource Conservation (INRES), University of Bonn, Bonn 53113, Germany

[2] Plant Genetics, TUM School of Life Sciences, Technical University of Munich, Freising 85354, Germany

[3] Crop Functional Genomics, Institute of Crop Science and Resource Conservation (INRES), University of Bonn, Bonn 53117, Germany

[4] Department of Plant Nutrition, College of Resources and Environmental Science, China Agricultural University, Beijing 100193, China

[5] Institute for Plant Sciences, Cologne Biocenter, Cluster of Excellence on Plant Sciences, University of Cologne, Cologne, Germany

[6] State Key Laboratory of Maize Bio-breeding, Frontiers Science Center for Molecular Design Breeding, Joint International Research Laboratory of Crop Molecular Breeding, National Maize Improvement Center, College of Agronomy and Biotechnology, China Agricultural University, Beijing 100193, China

[7] Max Planck Institute of Molecular Plant Physiology, Potsdam 14476, Germany

[8] State Key Laboratory of Plant Physiology and Biochemistry, College of Biological Sciences, China Agricultural University, Beijing 100193, China

[9] Molecular Plant Nutrition, Leibniz Institute of Plant Genetics and Crop Plant Research (IPK), Gatersleben 06466, Germany

[10] State Key Laboratory of Nutrient Use and Management, Frontiers Science Center for Molecular Design Breeding, College of Resources and Environmental Sciences, China Agricultural University, Beijing 100193, China

[11] Center for Crop Functional Genomics and Molecular Breeding, China Agricultural University, Beijing 100193, China

[12] Institute of Nutritional and Food Sciences, Food Microbiology and Hygiene, University of Bonn, Bonn 53115, Germany

[13] Faculty of Biology, Genetics, LMU Munich, Planegg-Martinsried 82152, Germany

[14] Shanghai Key Laboratory of Bio-Energy Crops, School of Life Sciences, Shanghai University, Shanghai, 200444, China

[15] Sanya Institute of China Agricultural University, Sanya 572025, China.

[#] These authors equally contributed to this work.

[*] To whom correspondence should be addressed:

[*] steve@cau.edu.cn, [**] hochholdinger@uni-bonn.de, [***] pengyu.yu@tum.de (lead contact)

Summary

Efficient nutrient acquisition in crops depends on coordinated interactions between plant roots and associated microbiota. Arbuscular mycorrhizal (AM) fungi enhance root system plasticity, yet the underlying regulatory mechanisms remain incompletely understood. Here, we investigate AM fungus–induced lateral root development in maize (*Zea mays*) and identify ethylene-responsive transcription factors (ERFs) as key regulators of pericycle cell division. ERF activity is associated with ethylene biosynthesis genes *ACS6* and *ACS7* and is required for AM fungus–stimulated lateral root formation. We further observe that AM colonization is accompanied by shifts in flavonoid profiles, including reduced accumulation of flavonols such as kaempferol and quercetin. In addition, the rhizobacterium *Massilia* associates with fungal hyphae and displays context-dependent effects on root development. Together, these findings support a model in which ethylene signaling and ERF activity contribute to AM-induced root developmental responses, with flavonoid metabolism and hyphosphere-associated bacteria representing additional modulatory components.

Key words:

Arbuscular mycorrhizal fungi, *Massilia*, Ethylene response factor, Flavonoids, Lateral root, Maize, Pericycle

Introduction

Arbuscular mycorrhizal (AM) fungi form ancient and widespread mutualistic associations with most land plants, enhancing nutrient acquisition—particularly phosphorus—and contributing to plant stress resilience (Lanfranco et al., 2018). These obligate biotrophs rely on host-derived carbon while facilitating the uptake of mineral nutrients and water (Gutjahr and Parniske, 2013). In addition to plant–fungus interactions, AM fungi associate with diverse soil bacteria in the rhizosphere and hyphosphere, where these organisms can influence nutrient cycling, microbial community structure, and plant performance (Desirò et al., 2014; Xue et al., 2019; Duan et al., 2024). Although such multipartite associations are increasingly recognized, the extent to which host developmental programs integrate these interactions remains unclear.

The spatial organization of cereal root systems is critical for both soil resource acquisition and the establishment of mycorrhizal symbiosis (Hochholdinger et al., 2018; Yu et al., 2016). Early stages of AM colonization involve plant-derived strigolactones and fungal signaling molecules such as chitooligomers and lipochitooligosaccharides, which initiate cellular responses in host roots (MacLean et al., 2017). However, how these signals are translated into changes in root developmental trajectories, particularly in non-legume crops such as maize, remains insufficiently understood.

Flavonoids represent an important class of plant secondary metabolites implicated in root–microbe interactions. In addition to their established roles in legume–rhizobia symbiosis, flavonoids can influence AM fungal development and modulate rhizosphere microbial communities (Hassan and Mathesius, 2012; Tian et al., 2021; Cook et al., 2025). Certain flavonoids have been reported to affect fungal hyphal growth and to associate with the enrichment of bacterial taxa, including members of the genus *Massilia* (Yu et al., 2021; He et al., 2024; Zhao et al., 2024). These observations suggest that flavonoid metabolism contributes to shaping root-associated microbial assemblages, although the underlying regulatory connections to host developmental processes remain to be clarified.

Lateral root formation is a key determinant of root system plasticity and nutrient foraging capacity. In maize, lateral roots originate from phloem pole pericycle cells and are controlled by both auxin-dependent and auxin-independent pathways (Yu et al., 2016; Van Norman et al., 2013). The maize lateral rootless1 (*lrt1*) mutant lacks embryonic lateral roots but exhibits partial recovery of lateral root formation upon AM fungal inoculation (Paszkowski and Boller, 2002). This response appears to occur independently of canonical auxin redistribution, indicating the involvement of alternative regulatory pathways in AM-induced root development.

Here, we investigate the molecular basis of AM fungus–induced lateral root development in maize. We identify members of the ethylene-responsive transcription factor (ERF) family as regulators associated with pericycle cell division and AM-induced lateral root formation. ERF activity is linked to ethylene biosynthesis genes (*ACS6* and *ACS7*) and is required for the full lateral root response to AM fungal colonization. In parallel, we observe that AM colonization is accompanied by shifts in flavonoid profiles and the association of hyphosphere bacteria, including *Massilia*. Together, our results support a model in which ethylene

93 signaling and ERF activity contribute to AM-induced developmental responses, with flavonoid metabolism
94 and associated bacteria representing additional components influencing this process. These findings
95 provide a framework for understanding how host developmental programs interface with microbial
96 interactions during root system adaptation.

97

Results

Pericycle division competence is associated with stage-specific transcriptomic reprogramming during lateral root initiation

To investigate the molecular basis of lateral root initiation in maize, we compared the spatiotemporal pattern of pericycle cell division in the lateral root-deficient mutant *lrt1* and its wild type (WT). Histological analysis showed that in *lrt1*, pericycle cell divisions were arrested at stage II along the longitudinal developmental zone of the primary root, preventing the formation of lateral root primordia (Fig. 1A). To examine the transcriptional basis of this developmental arrest, we performed laser capture microdissection (LCM) of phloem-pole (PP) and xylem-pole (XP) pericycle cells at defined positions along the root axis (5–10 mm, 10–15 mm, and 15–20 mm from the root tip, corresponding to stages I–III; Fig. 1B), followed by RNA sequencing.

Principal component analysis (PCA) showed that pericycle cell identity (PP versus XP) explained the largest proportion of variance (PC1, 29.8%), whereas genotype (*lrt1* versus WT) accounted for an additional component of variation (PC2, 9.0%) (Fig. 1C). Within PP pericycle cells, WT samples displayed a clear transcriptional progression across developmental stages, whereas *lrt1* samples showed reduced separation between the later stages, consistent with impaired developmental progression. These observations indicate that lateral root initiation in maize is accompanied by stage-dependent transcriptomic reprogramming in PP pericycle cells and that this progression is altered in *lrt1*.

ERF transcription factors are associated with pericycle developmental progression during lateral root initiation

To identify transcriptional regulators associated with LRT1-dependent pericycle competence, we applied weighted gene co-expression network analysis (WGCNA) to the pericycle transcriptomes. This analysis identified 39 co-expression modules representing distinct expression patterns across developmental stages, cell types, and genotypes (Fig. 1D). Several modules were preferentially associated with PP pericycle cells undergoing developmental progression, whereas others were enriched in XP pericycle cells (Supplementary Fig. 1). Modules showing elevated expression in stage III WT PP cells coincided with the developmental window in which lateral root primordium formation becomes evident (Fig. 1A, D).

Gene Ontology analysis of PP-enriched modules identified overrepresented categories related to cell cycle progression, microtubule organization, and mitotic transition, consistent with cell division competence, whereas XP-enriched modules were associated with cell wall-related and hormone-responsive functions (Supplementary Table 1). Promoter motif analysis of selected PP-enriched modules revealed enrichment of a GCC-rich cis-element resembling known ethylene response factor (ERF) binding motifs (Fig. 1G; Supplementary Table 2). In addition, one co-regulated module was enriched for genes annotated with transcription factor activity, with ERF family members significantly overrepresented (Fig. 1E, F;

Supplementary Table 3). Five ERF genes displayed peak expression in WT PP cells at stage III (Fig. 1H), consistent with a potential role during lateral root initiation.

To further examine the association between ERF expression and lateral root phenotypes, we analyzed transcriptomes from dissected stele tissues of representative intermated B73 × Mo17 (IBM) recombinant inbred lines showing high or low lateral root density (Supplementary Fig. 2a–c). Differential expression analysis identified more than 1,100 genes, among which ERF and MYB transcription factor families were enriched in lines with higher lateral root density (Supplementary Fig. 2d–g). Although this analysis does not establish conservation across maize germplasm, it supports an association between ERF-related transcriptional programs and lateral root formation.

Finally, we generated CRISPR/Cas9 knockout lines for two ERF genes, *ereb97* and *ereb147*, which were among the ERF genes expressed in competent pericycle cells (Fig. 1I). Independent mutant alleles showed an approximately 30% reduction in lateral root density on the primary root relative to WT controls (Fig. 1J). Together, these results support a positive contribution of ERF genes to lateral root development in maize.

AM fungal inoculation promotes lateral root formation and is associated with ERF activation

To investigate whether AM fungal colonization influences lateral root development in *lrt1*, we inoculated mutant plants with the AM fungus *Rhizophagus irregularis* under phosphate-deficient substrate conditions. After 6 weeks, inoculated *lrt1* plants showed increased lateral root formation relative to non-inoculated controls (Fig. 2A), together with increased shoot biomass (Supplementary Fig. 3), indicating that AM fungal colonization partially alleviates the root developmental defect under low-phosphate conditions.

To examine the transcriptional basis of this response, we isolated pericycle cells at developmental stages I–III from WT and *lrt1* roots with or without AM fungal inoculation and performed RNA-seq. PCA indicated that AM fungal treatment was associated with a marked transcriptional shift in pericycle cells (Fig. 2B). Pairwise comparison between *lrt1* roots with and without AM fungal inoculation identified 1,855 differentially expressed genes ($|FC| \geq 2$; FDR ≤ 0.05), including 1,004 upregulated genes in inoculated roots (Supplementary Fig. 4). GO enrichment analysis highlighted transcription-related processes, and transcription factor family enrichment analysis identified ERF and Dof families among the induced groups (Fig. 2C).

Among the AM fungus-induced ERF genes, five overlapped with ERF genes showing altered expression in *lrt1* relative to WT (Fig. 2D). Consistent with a functional role, AM fungal inoculation did not increase lateral root density in *ereb97* and *ereb147* mutants to the same extent as in WT plants (Fig. 2E). These data indicate that ERF activity contributes to the lateral root response associated with AM fungal colonization.

We next assessed whether ERF mutations influenced AM fungal colonization. Total colonization rates in crown roots were not significantly different between WT and the ERF mutants (Fig. 2F). However, hyphal length density in the surrounding substrate was reduced in the mutants (Fig. 2G). Because the ERF mutants also showed reduced lateral root density, this reduction in extraradical hyphal development may reflect

altered root system architecture and/or host-associated effects on fungal growth. Overall, these findings indicate that ERF genes contribute to AM fungus-associated lateral root development, while having more limited effects on overall intraradical colonization as quantified here.

AM fungal colonization is accompanied by cortex-associated changes in flavonoid-related metabolism

To characterize metabolic responses associated with AM fungal colonization, we performed tissue-resolved metabolomic (UPLC-MS/MS) and proteomic (iTRAQ) analyses of stele and cortex tissues from *lrt1* roots with or without AM fungal inoculation (Fig. 3A). Partial least squares discriminant analysis revealed clear separation among tissues and treatments, consistent with tissue-specific metabolic responses to AM fungal colonization (Supplementary Fig. 6A). In total, 611 metabolites in the stele and 447 metabolites in the cortex were significantly altered after inoculation (VIP ≥ 1; FC ≥ 1.2 or ≤ 0.8; $q < 0.05$) (Supplementary Fig. 6B). Many metabolites showed lower abundance in inoculated roots relative to controls (Supplementary Fig. 6C).

ChemRICH analysis of cortex-derived metabolites indicated significant enrichment of flavonoid- and sesquiterpene-related classes (Fig. 3B). Multiple flavonoid subclasses, including flavonols, flavones, and their modified derivatives, were detected (Fig. 3C), indicating that AM fungal colonization is associated with substantial remodeling of flavonoid-related metabolism in the cortex. Because several of these compounds changed in abundance, these data suggest shifts in flavonoid pathway output, although the current dataset does not resolve flux through individual branches. Pathway reconstruction further highlighted flavonoid biosynthesis as one of the pathways most strongly associated with the cortex response to AM fungal colonization (Supplementary Fig. 7; Supplementary Table 4).

Proteomic analysis identified 163 differentially accumulated proteins in the cortex of *lrt1* following AM fungal inoculation (Fig. 3D). Among the annotated proteins, phenylpropanoid biosynthesis was among the enriched pathways, and several class III peroxidases accumulated to higher levels in inoculated roots (Supplementary Table 5). Together, these data indicate that AM fungal colonization is associated with coordinated changes in cortex-localized phenylpropanoid- and flavonoid-related metabolism.

To further examine the relationship between ERF-associated developmental defects and flavonoid accumulation, we quantified kaempferol and quercetin in *lrt1* and ERF mutant roots with or without AM fungal inoculation (Fig. 3E). In the absence of AM fungal inoculation, both *lrt1* and ERF mutant roots accumulated higher levels of kaempferol and quercetin than their respective WT controls. Upon AM fungal inoculation, the abundance of these compounds was reduced in both mutant backgrounds. These results are consistent with an association between AM fungal colonization and reduced flavonol accumulation, but they do not by themselves establish a direct regulatory link between ERF activity and flavonoid biosynthesis.

We next assessed AM fungal colonization in the flavonoid-rich maize inbred line C2 and its flavonoid-deficient mutant C2-idf. The C2-idf line differed from C2 in intraradical colonization, whereas hyphal length density in the surrounding substrate was not detectably altered under the conditions tested (Fig. 3F). These

data suggest that host flavonoid status may influence aspects of root colonization, although the direction and mechanistic basis of this effect require further clarification.

Host flavonoid status is associated with Massilia abundance and AM fungus-related responses

To explore whether host metabolic status is linked to rhizosphere bacterial composition, we analyzed the microbiome of *lrt1* and WT roots. Several bacterial taxa, including *Massilia*, *Pseudomonas*, and *Sphingobium*, differed in relative abundance between genotypes, whereas bulk substrate communities were less affected (Fig. 4A). These observations indicate that the *lrt1* root phenotype is associated with changes in root-associated bacterial assemblages.

Because previous work implicated *Massilia* in lateral root-associated responses (Yu et al., 2021), we further characterized representative isolates. Several *Massilia* strains, including R1485, produced indole-3-acetic acid (IAA) and formed biofilms in vitro (Supplementary Fig. 8). These properties are consistent with a potential capacity to influence root-associated processes, although they do not establish a direct mechanism for lateral root induction in the present system.

To test whether *Massilia* can associate with AM fungal hyphae, we used a bi-compartment system that physically separated roots from a hyphal-only compartment (Fig. 4B). Microscopy indicated that strains R1485, I317, and Ox6 were present on actively growing *R. irregularis* hyphae and formed visible aggregates along the hyphal surface (Supplementary Fig. 9). In contrast, the non-beneficial strains tested, as well as heat-treated bacterial preparations, showed much weaker or no detectable association under the same conditions (Fig. 4C; Supplementary Fig. 9). These results support selective association of particular *Massilia* strains with AM fungal hyphae, although stronger evidence for stable attachment would require additional washing-based or quantitative assays.

We next tested whether host flavonoid status influenced *Massilia*-associated plant responses. In the flavonoid-rich genotype C2, *Massilia* inoculation was associated with greater shoot growth than in the flavonoid-deficient mutant C2-idf (Fig. 4D), and qPCR indicated higher *Massilia* abundance in the rhizosphere of C2 than of C2-idf plants (Fig. 4E). Under the same conditions, *Massilia* treatment was associated with altered AM fungal colonization and hyphal length density in C2, whereas these responses were less evident in C2-idf (Fig. 4F, G). Because some treatments showed limited statistical separation, these results are most consistent with the conclusion that host flavonoid status influences the context in which *Massilia* and AM fungal responses are observed, rather than demonstrating a strict gating mechanism.

ACS6/7-dependent ethylene biosynthesis contributes to ERF activation and AM fungus-associated root responses

To place ethylene biosynthesis in this pathway, we analyzed *acs6* and *acs7* loss-of-function mutants together with ACS6 and ACS7 overexpression or promoter lines. In WT maize, AM fungal inoculation increased the expression of *ERF97* and *ERF147*, whereas this induction was attenuated in *acs6* and *acs7*

mutants (Supplementary Fig. 10A, B). Conversely, ACS overexpression and promoter lines showed higher expression of these ERFs than WT. These data indicate that ACS6/7-dependent ethylene biosynthesis promotes, but is not solely required for, AM fungus-associated ERF activation.

Consistent with this trend, AM fungal inoculation was associated with reduced lateral root and fungal response phenotypes in *acs* mutants and enhanced responses in ACS overexpression backgrounds (Supplementary Fig. 10C, D). These observations support a role for ACS6/7-dependent ethylene biosynthesis in modulating AM fungus-associated developmental responses.

To further assess the interaction between ethylene status and *Massilia*-associated responses, we co-inoculated ACS7-OE and *acs7-1* plants with *Massilia* and AM fungus. ACS7-OE plants showed greater shoot growth than WT or *acs7-1* under some co-inoculation conditions (Fig. 5A). Measurements of AM fungal colonization and hyphal length density showed genotype- and treatment-dependent variation, with the clearest differences observed in combined inoculation treatments rather than in *Massilia*-only treatments (Fig. 5B, C). qPCR indicated that ACS7-OE roots supported higher *Massilia* abundance than WT or *acs7-1* in these experiments (Fig. 5D). By contrast, exogenous ACC or AVG treatment did not visibly alter *Massilia* biofilm formation on fungal hyphae in the compartment assay (Fig. 5E), suggesting that the contribution of ethylene signaling is more likely mediated through host root status than through a direct effect on bacterial attachment under these conditions.

Across ACS-related genotypes, the allelic effects were associated with lateral root density, shoot biomass, and shoot phosphorus accumulation under co-inoculated conditions (Fig. 5F, G; Supplementary Fig. 11A, B). Taken together, these data support a model in which ACS6/7-dependent ethylene biosynthesis contributes to ERF activation and influences AM fungus-associated root developmental responses, while flavonoid-related metabolism and *Massilia* association represent additional context-dependent components of this system (Fig. 6).

Discussion

AM fungal colonization is associated with changes in maize root developmental responses

Our study links maize lateral root development with transcriptional and metabolic changes associated with arbuscular mycorrhizal (AM) fungal colonization. In the lateral root-defective mutant *lrt1*, AM fungal inoculation partially restored lateral root formation under low-phosphate conditions, indicating that AM colonization can influence host root developmental responses beyond its established role in nutrient acquisition. This observation is consistent with previous studies showing that AM fungi can alter root system architecture and developmental plasticity in response to nutrient limitation (Chiu et al., 2018, 2022; Zhang et al., 2024). At the same time, the partial nature of this rescue suggests that AM fungal colonization does not bypass the underlying developmental defect in *lrt1*, but instead modulates a subset of host processes associated with lateral root formation. Our cell-type-resolved transcriptomic analyses further showed that pericycle developmental progression is altered in *lrt1* and shifts substantially upon AM fungal inoculation. Within this response, members of the ERF transcription factor family were repeatedly associated with lateral root-forming tissues, AM-responsive transcriptional changes, and reduced lateral root density in mutant backgrounds. Together, these observations support the view that ERF-associated transcriptional programs contribute to the host developmental response accompanying AM fungal colonization in maize.

Consistent with previous studies (Sun et al., 2025; Wang et al., 2025), our dual-compartment and co-inoculation experiments indicate that *Massilia* spp. can associate with AM fungal hyphae and are linked to changes in hyphal growth and colonization patterns under conditions where host-derived flavonoids are present (Fig. 4). These observations suggest that specific root-associated bacteria may contribute to AM fungus–associated responses depending on the chemical and developmental context established by the host, rather than acting independently. This interpretation is in line with recent work showing that AM fungi interact with structured hyphosphere microbiomes, often enriched in bacterial taxa such as *Devosia*, *Streptomyces*, and *Pseudomonas*, which can influence nutrient cycling and root colonization processes (Wang et al., 2022; Li et al., 2023; Jin et al., 2024; Zhang et al., 2024). Together, these findings support the view that the root–soil interface reflects the combined contributions of host developmental state, fungal colonization, and associated bacterial communities, rather than the action of individual microbial taxa alone.

Flavonoids are associated with metabolic and microbial changes during AM fungal colonization

Flavonoids are well-established plant secondary metabolites involved in root–microbe interactions, including roles in legume–rhizobia signaling and in modulating arbuscular mycorrhizal (AM) fungal development (Wang et al., 2022; Bouwmeester et al., 2025). Specific compounds, such as daidzein, naringenin, and sakuranetin, have been reported to influence AM fungal spore germination, hyphal growth, and colonization processes (Scervino et al., 2005; Buee et al., 2000; Lidoy et al., 2023). In line with these observations, our multi-omics analyses indicate that AM fungal colonization is associated with substantial changes in flavonoid-related metabolism in maize roots, particularly affecting quercetin- and luteolin-derived compounds in cortex tissues (Fig. 3). These changes are consistent with a remodeling of flavonoid

profiles during AM symbiosis, although the current data do not resolve whether they result from altered biosynthetic flux, transport, or microbial utilization.

Our results further suggest that host flavonoid status is linked to variation in AM fungal colonization and in the abundance of associated bacteria such as *Massilia*. In the flavonoid-deficient C2-idf mutant, differences in root colonization were observed relative to the flavonoid-rich C2 line, whereas hyphal density in the surrounding substrate was not markedly affected under the conditions tested. In addition, *Massilia*-associated effects on plant and fungal responses were more apparent in the flavonoid-rich background than in the mutant. These observations are consistent with the idea that flavonoids contribute to shaping the interaction context at the root–fungus–bacterium interface. However, they do not support a strict gating mechanism or demonstrate that flavonoids alone determine microbial recruitment or symbiotic outcomes.

Overall, our findings support a role for flavonoid-related metabolism as one component associated with AM fungus–induced root responses and with variation in root-associated microbial assemblages. Rather than acting as central coordinators of interkingdom communication, flavonoids are more appropriately viewed here as context-dependent chemical factors that may influence both fungal behavior and bacterial associations during root system adaptation.

ERF transcription factors are associated with developmental and AM fungus–related responses

At the transcriptional level, members of the ERF (ethylene response factor) family are implicated in both root development and responses to environmental and microbial signals (Cai et al., 2014; Das et al., 2025). Using laser capture microdissection, co-expression analysis, and mutant approaches, we identified ERF genes (including *ERF97* and *ERF147*) that are associated with pericycle developmental progression during lateral root initiation (Fig. 1). These ERFs showed stage-specific expression in phloem-pole pericycle cells and were reduced in the *lrt1* background. Loss-of-function mutants exhibited decreased lateral root density and showed a reduced lateral root response following AM fungal inoculation, supporting a role for ERF activity in these processes.

Our data further indicate that ethylene biosynthesis contributes to ERF activation in this context. Expression of *ERF97* and *ERF147* increased upon AM fungal inoculation in wild-type plants and was attenuated in *acs6* and *acs7* mutants, while elevated in ACS overexpression lines (Fig. 5; Supplementary Fig. 10). These observations are consistent with a model in which ACS6/7-dependent ethylene biosynthesis promotes ERF activation during AM-associated root responses. However, because AM fungal effects were not completely abolished in *acs* mutants, ethylene signaling is likely one of several contributing pathways rather than a sole determinant.

Although ACS-related genotypes also showed variation in lateral root density, shoot performance, and bacterial abundance under co-inoculation conditions, the present data do not establish a direct causal link between ERF activity and microbial recruitment. Instead, ERFs appear to function as components of the host transcriptional program associated with lateral root development and AM fungus–induced responses.

This interpretation is consistent with previous work indicating that ethylene-related pathways contribute to microbiota-responsive root architecture (Gonin et al., 2023), and more broadly with studies highlighting the role of host transcriptional regulation in shaping root-associated microbial interactions (Stringlis et al., 2018; Yu et al., 2021; He et al., 2024).

Conclusion

This study links host developmental regulators (LRT1, ERFs), ethylene biosynthesis (ACS6/7), and flavonoid-associated metabolism with root responses to arbuscular mycorrhizal colonization and associated microbial communities in maize. Our results indicate that ERF-related transcriptional programs contribute to lateral root development and to the host response accompanying AM fungal colonization, while ethylene signaling and flavonoid profiles are associated with variation in these processes. Rather than defining a complete mechanistic network, these findings provide evidence that root development, secondary metabolism, and microbial interactions are interconnected during plant adaptation to nutrient-limited conditions. This work offers a framework for future studies aimed at dissecting causal relationships within the root–microbiome system and for exploring strategies to improve crop performance through targeted manipulation of root traits and associated microbial interactions.

Resource availability

Lead contact

Requests for further information and resources should be directed to Peng Yu (pengyu.yu@tum.de).

Materials availability

Unique genetic resources and mutants generated in this study are available from the lead contract upon reasonable request.

Data and code availability

- Raw plant LCM cell RNA-seq data reported in this paper were deposited in the Sequence Read Archive (http://www.ncbi.nlm.nih.gov/sra) under accession no. PRJNA1366082.
- This paper does not report any original code.
- Any additional information required to reanalyze the data reported in this paper is available from the lead contract upon request.

Acknowledgements

We acknowledge Prof. Dr. Peter Dörmann from the Institute of Molecular Physiology and Biotechnology of Plants (IMBIO), University of Bonn, for providing mycorrhizal Ri T-DNA transformed carrot root organ culture to University of Cologne. We thank the Biocenter Imaging Facility of the University of Cologne and Dr. Parisa Kakanj for their support with microscopy performed on the Leica DMi8 Thunder Imager. We gratefully acknowledge the Center for Crop Functional Genomics and Molecular Breeding at China Agricultural University (CAU) for providing the ZmACS6 and ZmACS7 mutant and overexpression maize lines used in this study. This work is supported by the Deutsche Forschungsgemeinschaft (DFG) Emmy Noether Programme 444755415 to P.Y., research grants 514003603 and 552843484 to P.Y., the DFG Priority Program (SPP2089) 'Rhizosphere Spatiotemporal Organisation - A Key to Rhizosphere Functions' grant 403671039 to F.H. and P.Y., research grant HO 2249/12-2 to F.H. and the research group "FOR 5235: Cereal Stem Cell Systems (CSCS): Establishment, Maintenance and Termination" grant HO 2249/23-2 to F.H. This work was supported by the Biological Breeding-National Science and Technology Major Project (2024ZD04077) to X.L. Maize transformation was funded by Biological Breeding-National Science and Technology Major Project (2024ZD04077).

Author contributions

Conceptualization, P. Y. and F. H.; coordination and supervision, P. Y.; methodology, M. B., Y. Z., B. Y., L. G., X. H., M. B., N. von W., C.G., I. M., E. G., M. Bu. and P. Y.; investigation, M. Ba., Y. Z., B. Y., Y. A. T. M., S. W., Z. Z., L. Z., L. Y., and P. Y.; bioinformatics, T. T., F. H. and P. Y.; genetic resources, W. Q., R. S., I. M., E. G., M. Bu., X. L., F. H. and P. Y.; writing, C. L., X. L., F. H., and P. Y.; funding acquisition, X. L., F. H., and P. Y.

Declaration of interests

The authors declare no competing interests.

Supplemental information

Document S1. Figures S1–S11 and Table S1-S6

Materials and Methods

Plant Material and Germplasm Resources

The monogenic recessive maize root mutant *lrt1* (*lateralrootless 1*, Hochholdinger and Feix, 1998) and its corresponding wild type B73 were used. Moreover, homozygous naturally silenced maize *C2-Idf* (*Colorless2-inhibitor diffuse*) mutants and corresponding C2 wild type maize seeds were analysed (Della Vedova et al. 2005). In addition, we used recombinant inbred line (RIL) population derived from four generations of intermating of the inbred lines B73 and Mo17 (IBM) followed by seven rounds of selfing (Lee et al. 2002). Of the 163 RILs, 12 lines displayed a significantly distinct lateral root density. Among those the inbred lines 2033, 2043, 2156, 2215, 2242, 2274 displayed a low lateral root density) and the inbred lines 2088, 2104, 2161, 2162, 2168, 2236 displayed a high lateral root density. To generate the construct of CRISPR/Cas9-mediated knockout lines of *ZmACS6* and *ZmACS7* and perturbation of the C-terminal domain (PC) of *ZmACS7* editing, the specific 19-bp sgRNA (GTCGGAGCAACGTGGGTAC, TAAATGGCCGGTAGCAGCG, GAGATGGCGAGATGCGAAG) was cloned into the pBUE411 vector, respectively. To construct the overexpression lines of *ZmACS6* and *ZmACS7*, their full-length coding sequences were amplified from the cDNA of B73 and cloned into the pBCXUN vector to generate the *Ubi:ZmACS6* and *Ubi:ZmACS7* constructs. The knockout, PC, and overexpression lines of *ZmACS7* were used as previously described (Li et al., 2020). All seeds of the *ZmACS6* and *ZmACS7* transgenic lines were kindly provided by the Center for Crop Functional Genomics and Molecular Breeding of China Agricultural University. All primers were listed in Table S6. To the end, CRISPR-Cas9 knock out lines were generated for the maize genes *Zmereb97* and *Zmereb147* using the previously described simplex strategy (Qi et al. 2016). As a result the 47 bp sequence 5´ CCG AGG TAC CGC GGC GTC CGG AAG CGC CCC TGG GGA CGC TAC GCG GC 3´) sequence was deleted in the protein-coding region of *Zmereb97* and a 1 bp adenine was inserted in *Zmereb147*. The *Agrobacterium*-mediated maize transformation procedure was performed as described in the simplex strategy (Qi et al. 2016).

Experimental Set-up and Growth Conditions

For the phytochamber experiments, surface-sterilized seeds of the mutants *lrt1* and *C2-idf* and their corresponding wild type controls described above have been pre-germinated for three days in a paper roll system with deionized water in a 16-h-light, 26 °C, and 8-h-dark, 18 °C cycle. Germinated mutants and wild type seedlings with 2-3 cm length primary roots were transferred to new paper rolls and randomly distributed in a 5L beaker supplied with air and grown for another seven days. The same germination and cultivation procedures were applied to the 163 maize RILs used for phenotyping lateral root density.

For soil cultivation and inoculation with *R. irregularis*, 3-day pre-germinated mutants and wild type seedlings were transferred into an artificial soil containing sterilized coarse sand, fine quartz and loam (8:1:1 by weight) in a 2 L pot. For inoculation with *R. irregularis* (quality A spores from Agronutrition, Carbonne, France), the spore stock (2,000 spores per ml) were placed in a 50 ml Falcon tube and centrifuged at 3,000 x *g* for 10 min to spin down the spores. The supernatant (spore germination inhibition buffer) was removed and the

spores were washed three times with autoclaved AM water (50% tap water and 50 % deionized water) at 3,000 x *g* for 10 min. The final inoculants with 1,000 spores per plant were applied to the soil upon planting the 3-day-old seedlings. The plants were supplemented with modified Hoagland solution (Yu et al. 2015) with reduced phosphate (0.1 mM KH_2PO_4) and were grown 4-6 weeks in a well-controlled phytochamber with a 16-h-light, 26 °C, and 8-h-dark, 18 °C cycle.

For collecting the germinated AM fungal spores exudates, the stock spores in sterile AM water were placed in petri dishes to generate a large surface for air exchange and germinated at 30 °C for 14 days. During that time, the solution medium was corrected to the original volume due to evaporation. The germinated spores were checked under the stereomicroscope (Leica M165 FC) to confirm hyphae formation. The germinated spores were then centrifuged as described above and the supernatant of the germinated spore exudates were used to treat the recipient plants.

Soil Pot Experiments for Maize Ethylene Mutants

For soil culture experiments, the moderately acid soil (pH=6.36) which contained 4.24 mg olsen phosphorus (P) kg^{-1}, 0.29 g total nitrogen (N) kg^{-1}, and 27.02 mg exchangeable potassium (K) kg^{-1} was collected from Shangzhuang, Haidian, Beijing, China. Maize seeds of inbred lines B73-329 (WT), *ZmACS6* knockout (KO) and overexpression (OE) lines, *ZmACS7* (KO) knockout, overexpression (OE), and gain of function lines (PC) were germinated and grown in a pot with 1.8 kg of the low phosphorus soil, premixed with 200 mg kg^{-1} $(NH_4)_2SO_4$, 40 mg kg^{-1} KH_2PO_4, 200 mg kg^{-1} K_2SO_4, 50 mg kg^{-1} $MgSO_4$, 5 mg kg^{-1} $ZnSO_4$, 50 mg kg^{-1} $MnSO_4$, 5 mg kg^{-1} $CuSO_4$. 2 mL of the *R. irregularis* spore solution (42 spores mL^{-1}) was added to the soil for AM fungus inoculation treatment and the same volume sterilized water for the no-inoculation treatment. The seedlings were harvested after 8 weeks of soil culture. Crown root samples and the rhizosphere soil were collected and stored at -20℃ and -80℃ freezers for further analysis.

To further determine whether *Massilia* can promote maize growth under low phosphate conditions with AMF inoculation. Inbred lines B73-329 (WT), *zmacs7-1*, *ZmACS7-OE1*, *C2*, and *C2-idf* were inoculated with isolated strains including seven *Massilia*, thirteen *Telluria*, three *Collinonas*, two *Duganella*, and one *Pseudoduganella*. All strains were cultured overnight at 28°C in R2A liquid medium and then centrifuged for 10 min at 1,500 g. The pellets were resuspended in sterilized water and diluted to an optical density OD600 = 0.02, respectively. Before the inoculation experiment, the soil was sterilized with ^{60}Co γ-radiation to kill the soil-borne microbes with a dose of 20 kGy at Beijing Atomic High-tech Jinhui Radiation Technology Application Co. Ltd. Four treatments were set up, including sterile water, inoculation with the *Massilla* strain, inoculation with the *Massilla* strain and sterile water, and inoculation with the *Massilla* and nineteen other mixed strains treatments. We harvested the plants and soil samples at 8 weeks after soil culture for further analysis.The shoot samples were harvested for dry weight and P content analysis.

Dry Weight and P Content Measurement

The shoot samples were oven-dried at 105°C for 30 min to stop metabolic activity and then dried at 65°C until constant weight. After weighing the dry weight by using a balance, the samples were ground into a

455 powder and digested using H_2SO_4 and H_2O_2. Then digests were analyzed for P content by the
456 spectrophotometric colorimetric method (Soon and Kalra, 1995).

457 **Morphological, Histological and Anatomical Analyses of Lateral Root Initiation**

458 To determine lateral root density, primary roots of the mutants and the wild type plants together with the
459 RILs were dissected and the total emerged lateral root number was hand-counted. Lateral root density was
460 calculated as the number of emerged lateral roots divided by the length of the region where lateral roots
461 emerged.

462 Developmental stages of lateral root primordia were quantified from 4 cm long root segments from the root
463 tip of *lrt1* mutant seedlings and its wild type. In brief, 4 cm long primary roots were dissected into 5 mm
464 segments. These segments were then fixed and 10 µm longitudinal paraffin sections were prepared by a
465 rotary microtome (Leica) as described previously (Lim et al. 2000). Deparaffinized specimens were
466 gradually dehydrated then subjected to a acid-hydrolysis reaction with freshly prepared 1N HCl at room
467 temperature for 30 min. The hydrolyzed specimens were immediately dried with filter paper and stained by
468 Schiff's solution (Sigma) for 1 hour in the dark. The stained specimens were directly transferred to a freshly
469 prepared bleach solution (1N HCl, 10% $K_2S_2O_5$ and water with 1:1:18 ratio by volume) and were then
470 counterstained with Toluidine Blue (0.01% in water for 10-30 sec at room temperature). The stained
471 material wasthen dehydrated and embedded in Entellan (Merck) and analyzed under an AxioCam MRc
472 Microscope (Carl Zeiss Microimaging) and documented with Axio-Imager software (Carl Zeiss
473 Microimaging). The frequency of lateral root initiation was illustrated as the lateral root initiation index
474 (Dubrovsky et al. 2009) and lateral root primordia were further classified according to their developmental
475 stages (Malamy and Benfey 1997).

476 **Isolation of Pericycle Cell Types by Laser Capture Microdissection**

477 To understand the early events during lateral root initiation, pericycle cells adjacent to phloem and xylem
478 poles were isolated from cryosections as previously described (Yu et al. 2015). In brief, root segments at a
479 distance of 5-10 mm (Segment 1), 10-15 mm (Segment 2) and 15-20 mm (Segment 3) from the primary
480 root tip of *lrt1* and wild type seedlings were dissected and fixed immediately in a freshly prepared farmer's
481 fixative. After a series of vacuum infiltration/swirl and protecting/swirl steps, the root segments were
482 embedded in Tissue Freezing Medium and stored at -80°C until cryosectioning. The embedded molds with
483 root segments were cryosectioned in 20 µm sections using a Cryotome (Leica) at -28°C. The trimmed
484 cryosections were then mounted with PEN Membrane Slides (Carl Zeiss Microscopy). Prior to laser capture
485 microdissection (LCM), the tissue freezing medium was removed by sequential steps of dehydration with
486 ethanol and xylene solutions. LCM was performed on the air-dried sections with a PALM MicroBeam
487 Platform (Carl Zeiss Microimaging). Approximately ≥20 phloem-pole or xylem-pole pericycle cells were
488 isolated from each section and in total ca. 5,000 cells were pooled for each cell-type from respective 5 mm
489 root segment for downstream analysis. For the soil AM inoculation experiments, the same LCM work
490 pipeline was applied for crown roots of 4-week old *lrt1* plants with or without AM inoculation. In particular,

491 only phloem-pole pericycle cells were isolated from each section and in total around 15,000 cells were
492 pooled from respective 15 mm root segments for each mycorrhiza treatment.

493 **Physical Separation of Root Stele Tissues from IBM RILs**

494 The stele tissue contains the pericycle and is therefore enriched for cells involved in lateral root initiation.
495 To identify genes associated with lateral root formation, the stele tissues were manually separated from the
496 cortical parenchyma for the six RILs with high lateral root density and the six RILs with low lateral root
497 density (Reference). In brief, the first 5 mm of the root tip was removed from nine-day-old seedlings grown
498 in the paper roll system. Then the stele was separated manually from the cortical parenchyma in the root
499 region until the first lateral root emerged. Dissected stele tissues of 6-8 cm length were pooled from the
500 primary roots of ≥10individual plants for each RIL and stored at at -80 °C until RNA extraction.

501 **Isolation of RNA, cDNA Library Construction and Next Generation Sequencing**

502 RNA extraction from the LCM captured cells and the separated root steles were performed as previously
503 described (Yu et al. 2015, 2016). High quality RNA with RIN (RNA integrity number) values ≥6.5 were used
504 for downstream amplification and cDNA synthesis as previously described (Yu et al. 2016). cDNA library
505 construction, quantification and qualification of the sample libraries for Illumina sequencing were performed
506 as previously described (Yu et al. 2016). The raw sequencing reads were obtained by Illumina sequencing.
507 Subsequently, adapter sequences were trimmed and the quality score was checked using the FastQC
508 program. High quality sequencing reads were processed and subsequently mapped to the maize B73
509 reference genome sequence (RefGen_v3) with CLC Genomics Workbench software. Only reads uniquely
510 mapping to the reference genome were further analyzed. Prior to statistical analyses, data were normalized
511 by calculating FPKM (fragments per kilobase of exon per million fragments mapped) values by dividing the
512 total number of read pairs per gene by the product of mapped reads (millions) and exon length (in kb). Only
513 genes that were represented by a minimum of five mapped reads in all four replicates of at least one cell
514 type per segment per genotype were declared as expressed and considered for downstream analyses. The
515 raw sequencing reads were normalized by sequencing depth and were $\log_2$-transformed to meet the
516 assumptions of a linear model.

517 **Bioinformatics, Statistical Analyses of Sequencing Reads and Functional Characterization**

518 The homogenous distribution of replicated samples and thus the quality of the sequencing output of the
519 RNA-seq samples were determined by a principle component analysis (PCA) and hierarchical clustering
520 by CLC genomics workbench. The cell transcriptome data for two pericycle cell types across the three
521 segments between *lrt1* and its wild type were subjected to weighted gene co-expression network analyses
522 (WGCNA) to determine the gene co-expression modules across the 48 genotype-segment-cell type-
523 specific samples. Normalization, transformation and module detection was analysed as previously
524 described (Yu et al. 2020). Annotation of co-expressed genes within modules was performed by AgriGO.
525 Moreover, Fisher's exact test (Du et al., 2010) was applied to determine significant enrichment of

transcription factor families associated with the lateral root initiation. Furthermore, the CentriMo utility in MEME suite (Bailey et al. 2009) was used to perform transcription factor binding site enrichment analysis for WGCNA co-expressed module genes. We focused on the promoter regions as 1 kb upstream and 500 bp downstream of transcription start sites of co-expressed module genes after obtained the genomic sequences using a customized script. Within each module, 10 motifs with E-value less than 10^{-6} were recorded by MEME. Using the TOMTOM motif comparison tool, the resulting motifs were aligned with motifs in the JASPAR CORE Plants database (Mathelier et al. 2014) to identify significantly similar known *cis*-motifs (q-value < 0.05).

To identify the expression profile correlation and clustering among RILs with distinct lateral root densities, K-means clustering was performed with the K-means support module embedded in the MEV program with the figure of merit assessing the quality of the clustering algorithm (Yeung et al. 2001). Annotation of clustered genes was analyzed by AgriGO and association networks of the identified genes significantly enriched in GO terms were constructed with the aid of the online analysis tool STRING v10 (Szklarczyk et al. 2015).

To explore gene expression patterns after AM fungal inoculation, differential gene expression with or without AM fungal inoculation was performed by pairwise comparison for *lrt1* using the BIOCONDUCTOR package LIMMA (Smyth 2004) in R (v.3.1.1). Subsequently, we determined the number of differentially expressed genes for each comparison by controlling the *p*-values of the pairwise *t*-tests by adjusting FDR at 0.05 for multiple testing and a fold change |Fc| >2 (Benjamini and Hochberg 1995). Then, we functionally classified differential gene expression patterns according to Gene Ontology (GO) terms. The GO annotation system is based on three structured vocabularies that describe gene products in terms of their associated biological processes, cellular components and molecular functions in a species-independent manner. Subsequently, we performed a singular enrichment analysis to discover significantly overrepresented functional categories.

Integrated Proteome and Metabolome Analyses of Root Stele and Cortex with AM Inoculation

An integrated analysis of multiple types of omics data may improve the understanding of the molecular mechanism of root symbiosis with AM fungi. We first applied ultra-performance liquid chromatography-tandem mass spectrometry (UPLC-MS/MS)-based metabolomics to quantify the untargeted metabolites in AM-inoculated *lrt1* plants. Metabolites were extracted from an amount of 25 mg frozen tissue samples with 800 µL cold 50% methanol. These extracts were then fully lysed in a Tissue Lyser (40Hz, 5min). The lysed samples were precipitated at -80 °C for 2 h, then the extracts were centrifuged at 25,000×*g* for 15 min at 4 °C and 550 µL supernatant was transferred to a new vial. Prior to the UPLC/MS run, the quality control samples were used to calibrate the UPLC column. The quality control samples were also injected regularly throughout the run (after every 10 samples) to monitor the stability of the analytical platform. A high-resolution tandem mass spectrometer SYNAPT G2 XS QTOF (Waters, USA) was used for metabolite detection with ten biological replicates. Metabolic features alignment, peak extraction, normalization and

562 compound identification were performed by Progenesis QI (version 2.2). Moreover, quality control - based
563 robust LOESS (locally estimated scatterplot smoothing) signal correction (QC-RLSC) was applied to
564 efficiently correct the instrumental variation during metabolome analysis (Dunn et al. 2011). By combining
565 univariate and multivariate statistical analysis, significantly changed features (FDR <0.05, VIP ≥1, FC ≥1.2
566 or ≤0.8) were acquired and those significant features were further annotated with the databases PubChem
567 and KEGG. In addition, partial least squares - discriminant analyses (PLS-DA) were performed to maximize
568 the covariance of metabolic features of tissues upon inoculation with AM fungi.

569 To investigate the effects of AM inoculation on the metabolism of stele and cortex, isobaric tags for relative
570 and absolute quantitation (iTRAQ)-based proteome analysis was employed in parallel to investigate
571 proteomic changes of AM inoculated roots. Approximate 2 g frozen root tissues with 10%
572 polyvinylpolypyrrolidone were grounded into powder in liquid nitrogen and then sonicated on ice for 5 min
573 in lysis buffer (8 M urea and 40 mM Tris-HCl containing 1 mM phenylmethylsulfonyl fluoride, 2 mM EDTA
574 and 10 mM DTT, pH 8.5). Following centrifugation (25,000 *g*, 4 °C, 20 min), the supernatant was treated
575 by adding 5 volume of 10% trichloroacetic acid/acetone with 10 mM DTT to precipitate proteins at -20 °C
576 for 2 hours. The supernatant was discarded and the resulting pellet was washed twice with cold acetone
577 on ice. Prior to protein digestion, the concentrations of extracted proteins were quantified by a Bradford
578 assay using Coomassie Brilliant Blue G-250. Protein integrity was further determined by SDS-
579 Polyacrylamide Gel Electrophoretogram. Protein digestion was performed with Trypsin Gold (Promega,
580 Madison, WI, USA) at 37 °C overnight, followed by desalting of the peptides with a Strata X C18 column
581 (Phenomenex) and vacuum-drying. Afterwards, the peptides were labelled with the iTRAQ Reagent 8-plex
582 Kit according to the manufacturer's protocol (Applied Biosystems). The iTRAQ-labelled peptides were
583 subjected to strong cation exchange fractionation on a Shimadzu LC-20AB HPLC Pump system coupled
584 with a high pH RP column. The peptides were reconstituted with buffer A (5% ACN, 95% H_2O, pH 9.8) to 2
585 ml and loaded onto a column containing 5 µm particles (Phenomenex). The peptides were separated at a
586 flow rate of 1 mL/min with a gradient of 5% buffer B (5% H_2O, 95% ACN, pH 9.8) for 10 min, 5-35% buffer
587 B for 40 min, 35-95% buffer B for 1 min. The system was then maintained in 95% buffer B for 3 min and
588 decreased to 5% within 1 min before equilibrating with 5% buffer B for 10 min. Elution was monitored by
589 measuring absorbance at 214 nm, and fractions were collected every 1 min. The eluted peptides were
590 pooled as 20 fractions and each fraction was concentrated via vacuum centrifugation. The iTRAQ-labelled
591 samples were analyzed using a LC-20AD nano-HPLC instrument (Shimadzu, Kyoto, Japan). Then, the
592 peptides were eluted from trap column and separated by an analytical C18 column (inner diameter 75 µm)
593 packed in-house. Data acquisition was performed with a TripleTOF 5600 System (SCIEX, Framingham,
594 MA, USA) equipped with a Nanospray III source (SCIEX, Framingham, MA, USA), a pulled quartz tip as
595 the emitter (New Objectives, Woburn, MA) and controlled with software Analyst 1.6 (AB SCIEX, Concord,
596 ON). The raw MS/MS data was converted into MGF format by ProteoWizard tool msConvert, and the
597 exported MGF files were searched using Mascot (version 2.3.02) against maize UniProt protein database
598 (https://www.uniprot.org/proteomes/UP000007305). IQuant (Wen et al. 2014) was applied for quantitatively

analyzing the labelled peptides with isobaric tags. All differentially accumulated proteins with a false discovery rate (FDR) >1% were included in downstream analyses including Gene Ontology (GO) enrichment analyses, KEGG pathway analyses and cluster analyses.

Quantification of AM Colonization and Microscopic Imaging, and Hyphal Density in Soil

Representative primary and crown roots were collected from *lrt1* and its wild type plants 6 weeks post-inoculation with *G. intraradices*, along with crown roots from the mutants of *ZmACS6* and *ZmACS7* and the corresponding B73-329 wild type lines after 8 weeks of inoculation with *R. irregularis.* Roots were stained with trypan blue and mycorrhizal colonization was quantified with a modified grid-line intersect procedure (Paszkowski et al. 2006). In brief, the total root length colonization was determined by the total amount of fungus scored microscopically at 100 random points per root sample. We also performed the trypan blue staining to determine the hyphal length density in rhizosphere soil according to the previous method (Brundrett et al., 1994).

RNA Extraction and Quantitative real-time PCR

RNA extraction, cDNA synthesis and real time RT-PCR were performed as previously described (Yu et al. 2015). RNA was isolated from 100 mg of liquid nitrogen-ground root samples with Trizol reagent according to the manufacturer's instruction (Invitrogen). The quality and quantity of isolated RNA were determined using a NanoDriop Spectrophotometer (Thermo Fisher Scientific, Waltham, MA, United States). 1 g of total RNA was purified and reverse transcribed into cDNA using the PrimeScript™ RT reagent Kit (Takara, Kyoto, Japan). TB Green® Premix Ex Taq™ (Takara, Kyoto, Japan) was used to detect the relative gene expression with *ZmTublin* as the internal control by RT-qPCR in a CFX96 Touch Real-Time PCR Detection System (Bio-Rad). All primers were listed in Table S6.

DNA Extraction and RT-qPCR Analysis of *Massilia* Relative Abundance

The DNA extracted from 0.5 g rhizosphere soil was performed using FastDNA™ Spin Kit for Soil DNA Extraction followed by instructions (MP Biomedicals, Irvine, CA, United States). Then the relative abundance of *Massilia* was quantified by RT-qPCR with the universal bacteria 16S rRNA gene and *Massilia* specific 16S rRNA gene. The primers were 1048F (5'-GTGSTGCAYGGYTGTCGTCA-3')/1194R (5'-ACGTCRTCCMCACCTTCCTC-3') and F (5'-GGAGCGGCCGATRTCTGATTAG-3')/R (5'-ATTCTACCCCCCTCTGCCARAY-3') for the universal bacteria 16S rRNA gene and *Massilia* specific 16S rRNA gene, respectively.

Flavonoid Quantification in Maize Root Extracts

Approximately 5 mg of lyophilized and ground maize root powder was extracted twice with 1 mL 70% methanol (MeOH; LC–MS grade; Th. Geyer) containing 1% formic acid (FA; Biosolve), followed by one extraction with 1 mL absolute ethanol containing 1% FA. Each extraction consisted of vortexing (30 s), sonication for 15 min in cooled water (BANDELIN ultrasonic bath), and 2 h overhead shaking at 4°C. All extracts were centrifuged at 14,000 rpm for 30 min at 4°C, pooled into 5-mL tubes, and dried in a SpeedVac

at 40°C. Pellets were reconstituted in 100 µL 50% MeOH with 0.1% FA and transferred to LC–MS vials. Flavonoids were separated on an Acquity UPLC HSS T3 column (150 × 2.1 mm, 1.8 µm; Waters) with a guard column using water + 0.1% FA (mobile phase A) and acetonitrile (ACN; LC–MS grade; Th. Geyer) + 0.1% FA (mobile phase B). The gradient was: 10% B (0–1 min), 10–30% B (1–2 min), 30–75% B (2–5 min), 75–85% B (5–8 min), followed by rinsing and re-equilibration. The column temperature was 30°C, flow rate 0.3 mL min^{-1}, injection volume 5 µL. Samples were analyzed on the same Vanquish UHPLC–Q Exactive Plus HESI-MS platform under identical ion source settings as used for strigolactones. Full MS/ddMS² data were acquired for quantification and structural confirmation. Calibration curves (1–800 ppb) were prepared in 50% MeOH containing 0.1% FA using authentic standards of apigenin and luteolin (Extrasynthese, France) and quercetin and kaempferol (Carl Roth, Germany). Quantification used extracted ion chromatograms of $[M+H]^+$ ions fitted by a 1/x-weighted linear regression. The limit of quantification was 1 ppb. Compound identity was confirmed by agreement in retention time, exact mass, isotope pattern, and MS² spectra with authentic standards and a custom spectral library. Among quantified metabolites, apigenin was consistently detected above LOQ; kaempferol, luteolin, and quercetin were either absent or below 1 ppb. Concentrations are reported as µg g^{-1} dry weight.

IAA production assay of *Massilia* isolates

Indole-3-acetic acid (IAA) production was quantified using the Salkowski colorimetric assay as described by Gordon and Weber (1951). Bacterial isolates were grown overnight and the cell density was adjusted to an OD_{600} of 0.8–1.25 using fresh medium. Subsequently, 50 µL of the adjusted culture were inoculated into 5 mL of R2A medium supplemented with 100 mg L^{-1} L-tryptophan. Sterile dH_2O (50 µL) served as the blank control. All treatments were performed in triplicate. Cultures were incubated for 24 h at room temperature on a rotary shaker and then centrifuged to remove cells. For colorimetric determination of IAA, 1 mL of the culture supernatant was mixed with 1 mL of Salkowski reagent (35% HClO4 and 10 mM $FeCl_3$) incubated in the dark at room temperature for 30 min. Absorbance was measured at 530 nm. IAA concentrations were quantified using a standard curve prepared from a stock solution of 8 mg IAA in 100 mL methanol, followed by six consecutive twofold dilutions. During analysis, 1 mL of each standard solution was mixed with 1 mL of Salkowski reagent. The Salkowski reagent consisted of 25 mL dH_2O, 25 mL 70% $HClO_4$, and 1 mL 0.5 mol L^{-1} $FeCl_3$.

Detection of biofilm formation among *Massilia* isolates

The biofilm-forming potential of the tested *Oxalobateraceae* isolates was assessed in 96-well polystyrene microtiter plates, based on the method described by Kolari et al. (2003), with minor modifications. The optical density was adjusted to 0.08-0.125 with R2A. 200 µL of R2A were inoculated with 2 µL of the adjusted culture. Plates were incubated at 30 °C for 24 h under static conditions. After incubation, bacterial growth in the wells was first quantified by measuring the optical density at 600 nm. The wells were gently emptied and stained with 250 µL of crystal violet solution (4 g L^{-1} in 20% methanol) for 5 min. Excess stain was removed, and the wells were washed three times with distilled water. The bound dye was solubilized

by the addition of 300 µL ethanol. After incubation for 60 min at room temperature, absorbance was measured at 550 nm using a microplate reader (CLARIOstar, BMG Labtech). Blank values were subtracted from the absorbance values of the isolates. Biofilm formation was defined as absorbance values exceeding three times the standard deviation of the blank (n = 4).

ACC deaminase activity analysis

ACC deaminase activity of the isolates was assessed using a growth-based assay modified from Koo et al. (2010). Briefly, overnight cultures were washed twice with Ringer solution and adjusted to an OD_{600} of 0.8–1.25. Aliquots (50 µL) of the adjusted cell suspensions were inoculated into DF minimal medium supplemented with 3 mM 1-aminocyclopropane-1-carboxylate (ACC) as the sole nitrogen source. DF medium containing ammonium sulfate served (2g/l) as a positive growth control, while DF medium without a nitrogen source was used as a negative control. Cultures were incubated at 30 °C for 3–5 days under shaking conditions (150 rpm). Bacterial growth was monitored by measuring OD_{600}, and isolates showing growth in DF medium supplemented with ACC were considered ACC deaminase positive.

Microscopic Analysis of Spatial Interactions Between AM Fungi and *Massilia*

Rhizophagus irregularis DAOM 197198 was maintained in an axenic *in vitro* system together with a Ri T-DNA-transformed carrot (*Daucus carota*) root organ culture in bi-compartmented Petri plates, with one compartment containing the root organ culture and the other supporting the growth of extraradical hyphae. Both compartments were filled with MSR medium (Cranenbrouck et al., 2005). Cultures were incubated in the dark at 25 °C until AM fungal hyphae covered at least 50% of the hyphal compartment‘s surface. Roots crossing the barrier were trimmed regularly to ensure that only extraradical hyphae colonized the hyphal compartment (St-Arnaud et al., 1996). Subsequently, 10 µl of a *Massilia* strains (R1485, I317 or I20) and Collimonas (Ox6) that had been grown in R2A medium (OD_{600} = 0.6) was applied to five different locations on the hyphal compartment. *E. coli* or heat-killed bacteria, autoclaved twice at 121 °C for 20 min, were used as controls. 72 hours after bacterial inoculation, bacterial attachment to fungal hyphae was analyzed using a Leica DMi8 Thunder Imager. Images were captured with a 63× objective and processed using LasX software (Version 3.10.0). Additionally, to qualitatively assess the frequency and relative intensity of biofilm formation across hyphal networks, images were acquired using a Leica DM1000 LED microscope at 10× magnification.

To assess the *Massilia* attachment to fungal hyphae under 1-aminocyclopropan-1-carboxylic acid (ACC) and aminoethoxyvinylglycine (AVG) (Sigma-Aldrich) supplementation, a 10 µM ACC or AVG working solution was prepared and applied to the agar surface (5 µL, four replicate spots per plate). On the same day as the ACC/AVG treatment, *Massilia* was inoculated into the hyphal compartment as described above, and biofilm formation was assessed after 72 hours.

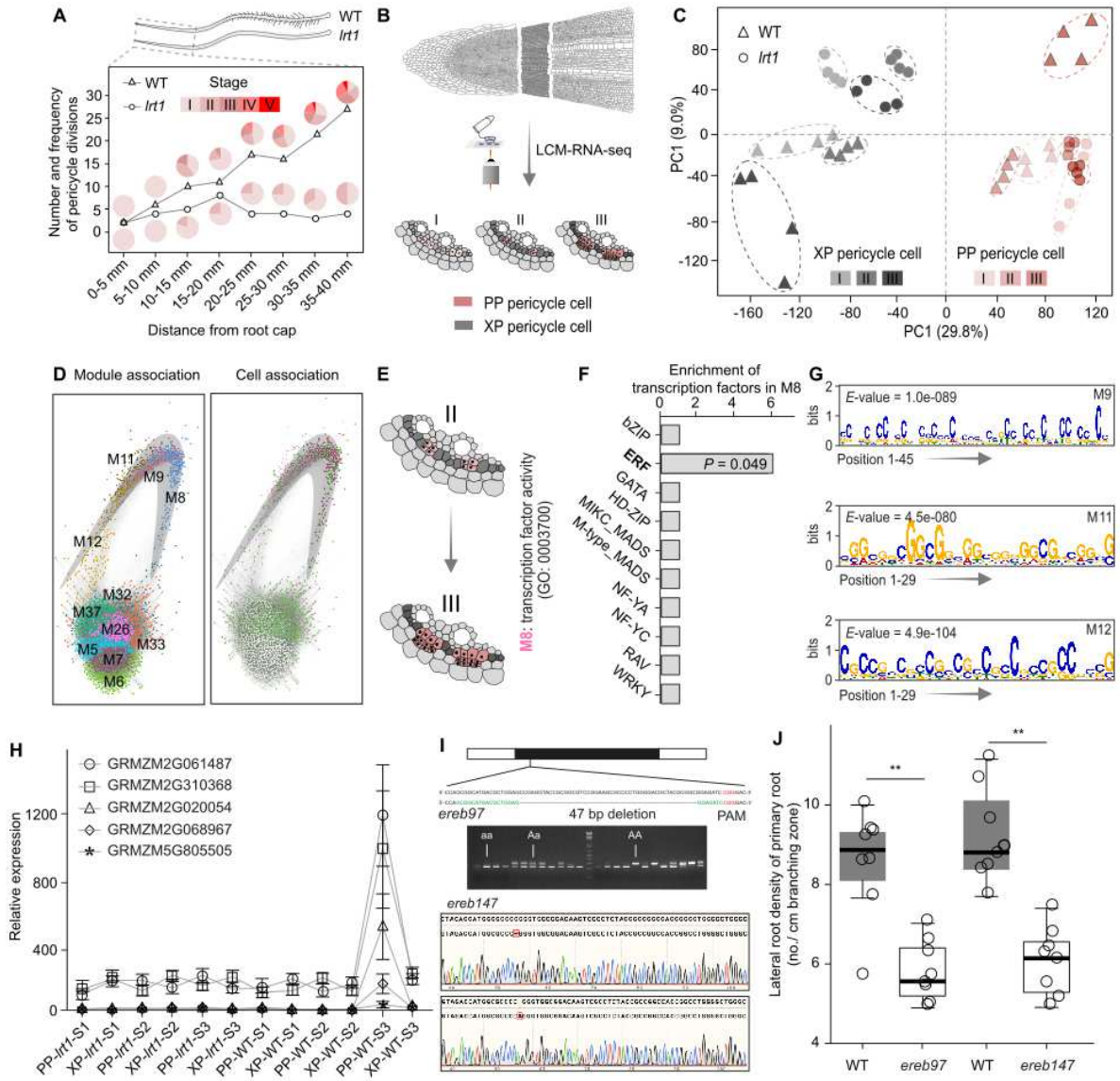


Figure 1. Ethylene response factors – mediated transcriptional regulation of lateral root initiation in maize.

(**A**) Developmental stages of lateral root formation in the maize *lrt1* mutant and wildtype. Relative proportion of developmental stages of lateral root primordia observed in 10-day-old maize seedlings of the wild-type B73 and the mutant *lrt1*. Primordia were examined and counted from paraffin sections using at least 6 plants for each genotype. Developmental stages nomenclature of maize lateral root was according to Yu et al., 2016. (**B**) RNA-seq analysis of stage-dependent phloem pole (PP) and xylem pole (XP) pericycle cells isolated by laser capture microdissection (LCM). Pericycle cell types were captured from the same cryo-sections to have highly accurate comparison. The detailed procedure of LCM was described in the Methods. (**C**) Principal component analysis (PCA) for pericycle cell transcriptomes from different developmental stages of maize *lrt1* mutant and wildtype. *n* = 4 biologically independent samples collected from at least 25 continuous cryo-sections per sample. (**D**) Gene module network and cell trait associations by weighted gene co-expression network analysis (WGCNA) and Spearman correlation coefficient (SCC) analysis. Different gene modules were indicated by different colour codes. Module eigengene expression

was correlated with lateral root initiation status of *lrt1* mutant and wildtype and clustered from green (SCC = 0) to pink (SCC = 1). (**E**) Identification and characterization of gene module 8 in association with pericycle cell developmental transition from stage II to stage III. Significantly (FDR adjusted *P* = 0.047) enriched gene ontology (GO) term is annotated into “transcription factor activity” (GO:0003700). (**F**) Statistically enrichment analysis of different transcription factor families in module 8 based on the maize transcription factor background (https://planttfdb.gao-lab.org/). Significant *P* value was corrected by FDR correction. ERF, ethylene response factor. (**G**) Gene motif enrichment analysis for M8 coregulated modules (M9, M11 and M12). Gene promoter region was extracted and subjected to MEME for detecting significantly enriched putative binding motif by CentriMo. Significant enrichments were measured by *E*-value applying Bonferroni correction to the term's *P*-value. (**H**) Relative expression of ERF genes during lateral root development in maize *lrt1* mutant and wildtype. PP, phloem pole; XP, xylem pole; S, stage. (**I**) Production of ERF mutants via CRISPR/Cas9. PAM, protospacer-adjacent motif. (**J**) Lateral root density phenotype of *ereb97* and *ereb137* mutants. n = 8. Statistical significance was controlled by paired Student’s *t* test.

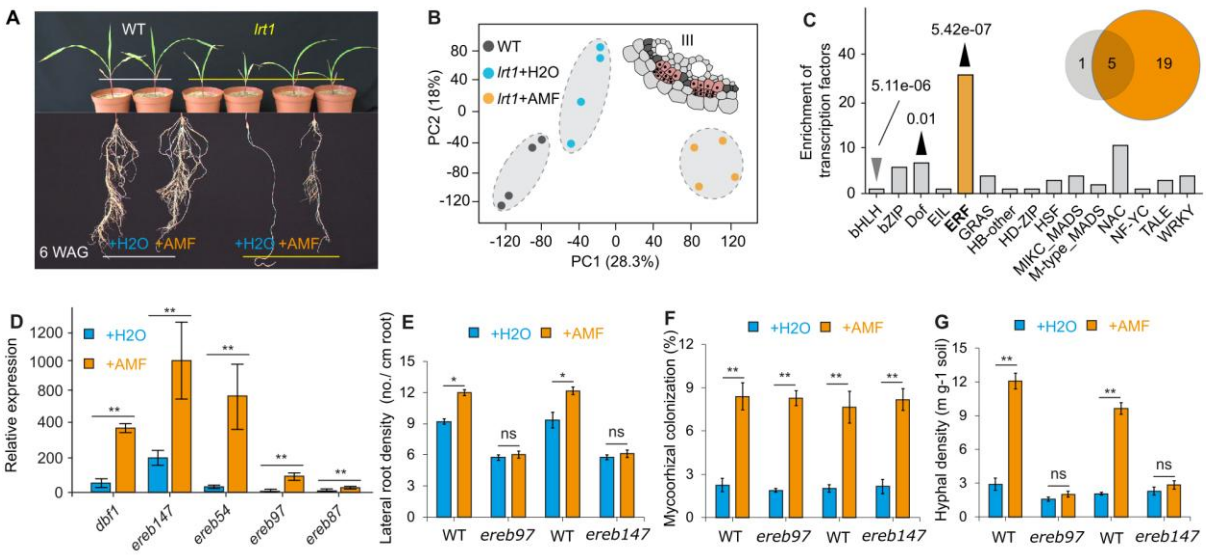


Figure 2. ERF transcription factors coordinate AMF-induced lateral root induction and rhizosphere hyphal expansion in maize. (**A**) AM inoculation recovered lateral root formation in the *lrt1* mutant. (**B**) AM inoculation largely reshaped the pericycle cell transcriptome. Here the stage III of the pericycle cells were captured and analysed by RNA-seq. (**C**) Enrichment analysis of transcription factors families. Statistical significance was controlled by chi-square test. An embedded Venn diagram indicates the overlapped transcription factors that AM fungi induced and the ones LRT1 silenced. (**D**) Relative expression of ERF genes in *lrt1* mutant induced by AM inoculation. Statistical significance was controlled by paired Student's *t*-test. (**E**) AM mediated lateral root formation depends on function of ERF genes (erf mutant has no lateral root induction by AMF). (**F**) ERF mutation does not affect the AM fungal colonization, but hyphal branching in the rhizosphere (**G**).

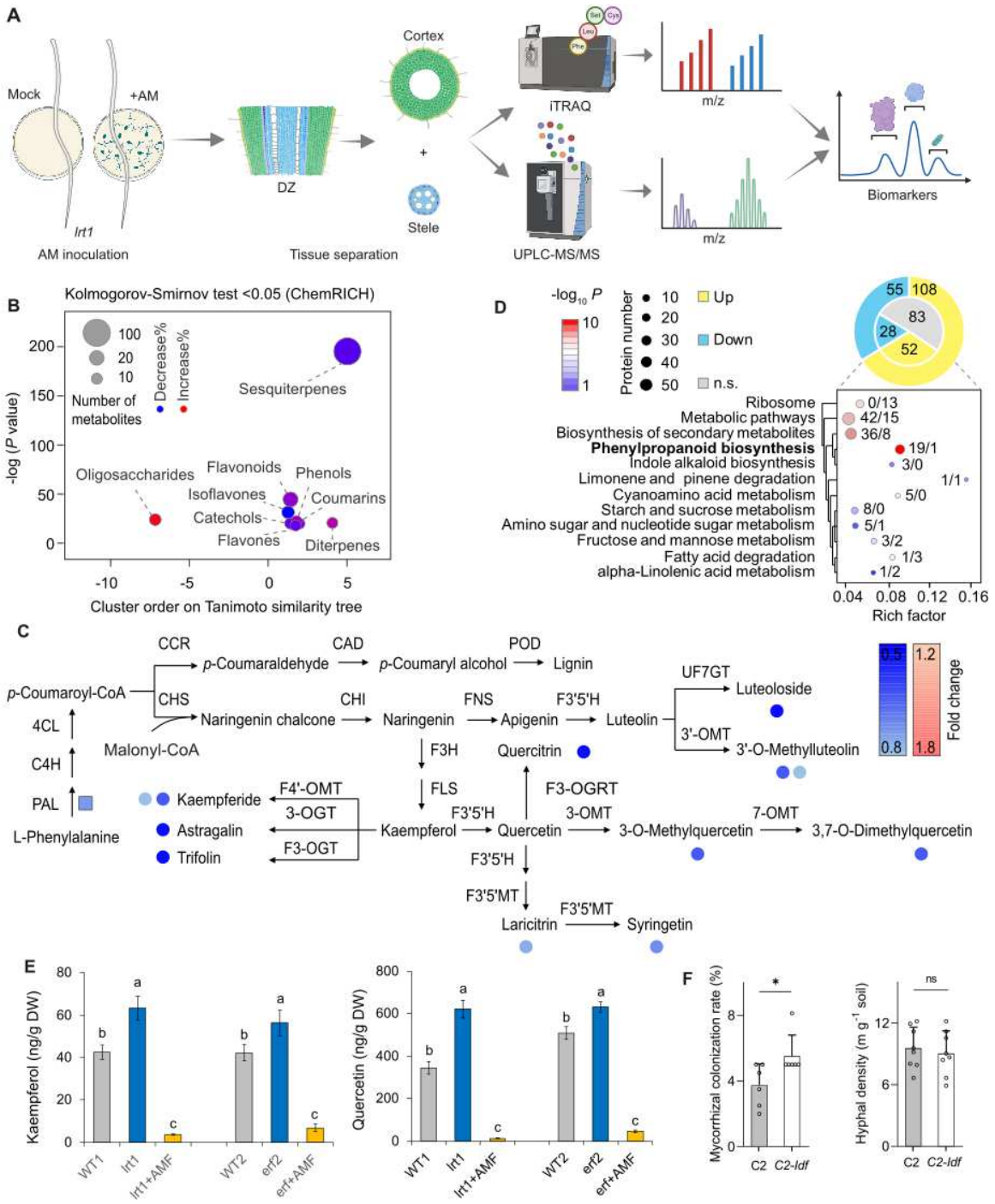


Figure 3. AM inoculation associated with host tissue-specific flavonoids homeostasis.

(**A**) Schematic steps and workflow of root tissue-specific proteomic and metabolic analyses involved into AM symbiotic processes of *Irt1* mutant. (**B**) AM fungal inoculation significantly altered metabolite accumulation in the root cortex of *Irt1*, highlighting specific metabolic reprogramming in association with flavonoids. (**C**) AM symbiosis reshaped the flavonoid biosynthesis pathway, with differential regulation of key enzymatic steps including CHS, CHI, FLS, F3H, and various O-methyltransferases and glycosyltransferases. 3-OGT: flavonol 3-O-glucosyltransferase; 3'OMT: flavone 3'-O-methyltransferase; 3-OMT: quercetin 3-O-methyltransferase; 4CL: 4-coumarate-CoA ligase; 7-OMT: 3-methylquercetin 7-O-

methyltransferase; C4H: cinnamate 4-hydroxylase; CAD: cinnamyl alcohol dehydrogenase; CCR: cinnamoyl-CoA reductase; CHI: chalcone isomerase; CHS: chalcone synthase; F3'5'H: flavanoid 3',5'-hydroxylase; F3'5'MT: flavonoid 3',5'-methyltransferase; F3H: flavanone 3-hydroxylase; F3-OGRT: flavonol-3-O-glucoside L-rhamnosyltransferase; F3-OGT: kaempferol 3-O-galactosyltransferase; F4'-OMT: kaempferol 4'-O-methyltransferase; FLS: flavonol synthase; FNS: flavone synthase; PAL: phenylalanine ammonia-lyase; POD: peroxidase; UF7GT: flavone 7-O-beta-glucosyltransferase. (**D**) Proteomic analysis revealed significantly accumulated proteins and associated Phenylpropanoid biosynthesis pathway enrichments in response to AM colonization. (**E**) AM inoculation suppressed excessive flavonoid accumulation in both *lrt1* and *erf* mutants, indicating that the AM symbiosis modulates host secondary metabolism even in regulatory mutants. Statistical significance was assessed using one-way ANOVA, and different letters indicate significant differences among genotypes. Differences among groups were analyzed using one-way ANOVA followed by Tukey's honestly significant difference (HSD) test. Different letters indicate statistically significant differences between groups ($P < 0.05$). Data are presented as mean ± s.e.m. (**F**) In contrast, the flavonoid-overproducing mutant C2 exhibited inhibited AM colonization despite high hyphal density in the rhizosphere, suggesting that excessive flavonoids may restrict fungal entry but not external fungal growth. Statistical significance was evaluated using a one-sided Student's t-test. * indicates *P* value < 0.05, ns, not significant.

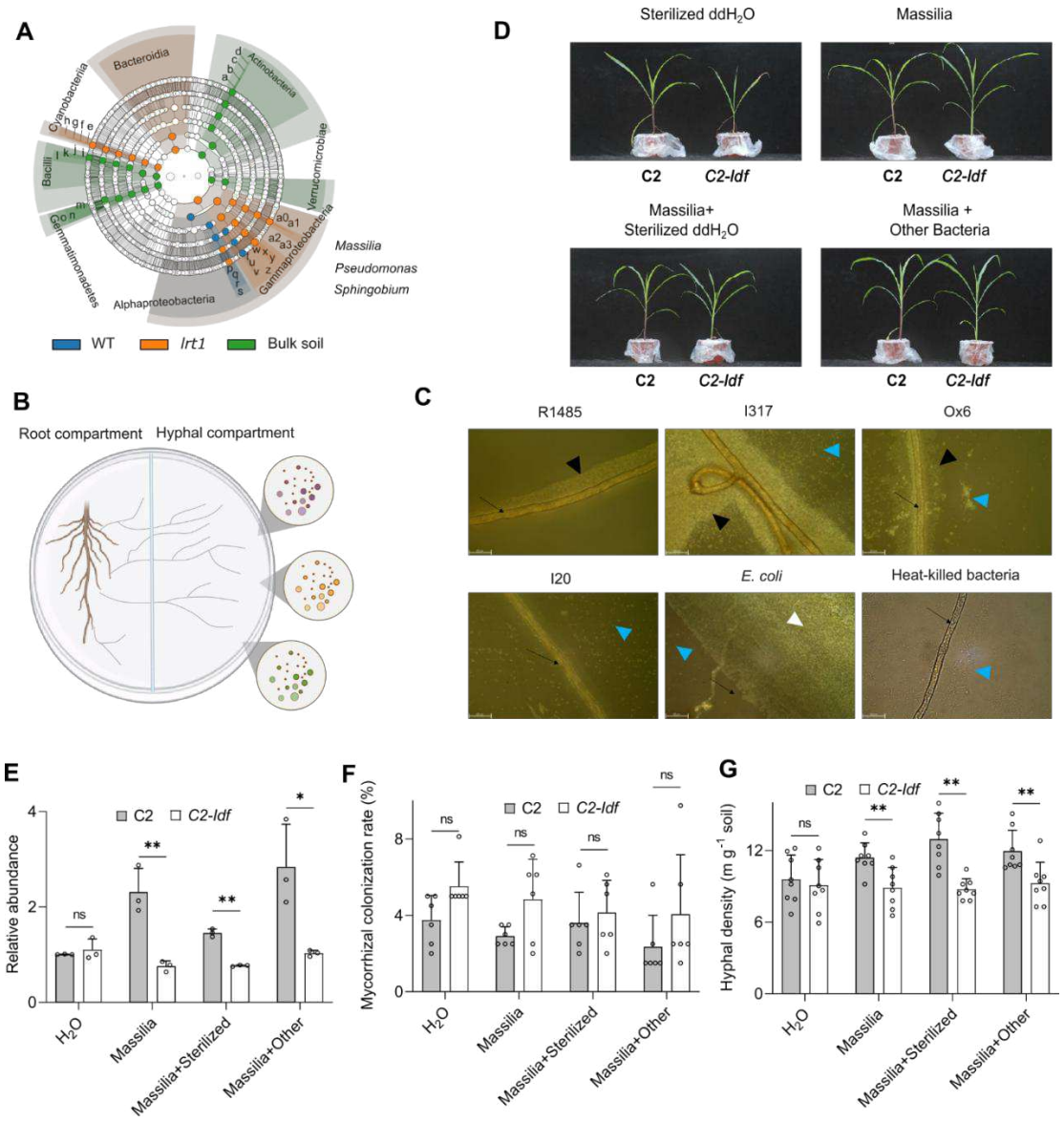


Figure 4. Host flavonoid status is associated with *Massilia* abundance and its interaction with AM fungal hyphae in the maize rhizosphere. (A) *Massilia* is selectively enriched in the rhizosphere of the *lrt1* mutant under low-phosphorus conditions, indicating a potential symbiotic association. **(B)** Schematic representation of an in vitro dual-compartment system used to study the interaction between AM fungal hyphae and *Massilia* colonization. **(C)** *Massilia* colonization along specific sectors of AM fungal hyphae taken close to the bacterial inoculation spot, visualized using a Leica DMi8 Thunder Imager. Hyphae are indicated by black arrows, bacterial inoculation spots by white triangle, free bacteria by blue triangles and bacterial biofilms by black triangles. **(D)** Growth response of wild-type maize (C2) and its flavonoid-deficient mutant (*C2-ldf*) upon inoculation with either individual *Massilia* isolates or *Massilia*-based synthetic communities. **(E)** Host-derived flavonoids significantly enhance *Massilia* enrichment in the rhizosphere. n = 3 biologically independent replicates. **(F)** Mycorrhizal colonization rates remain unchanged between genotypes and treatments. n = 6 biologically independent replicates. **(G)** Flavonoids also promote increased AM hyphal length density in the rhizosphere. n = 8 biologically independent replicates. For E,F and G, pairwise comparisons between genotypes (C2 vs *C2-idf*) were performed within each treatment using two-sided Student's *t*-tests. P values were adjusted for multiple comparisons using the Benjamini–Hochberg

false discovery rate (FDR) correction. Data are presented as mean ± SD; dots represent biological replicates. ns, not significant; *P < 0.05; **P < 0.01.

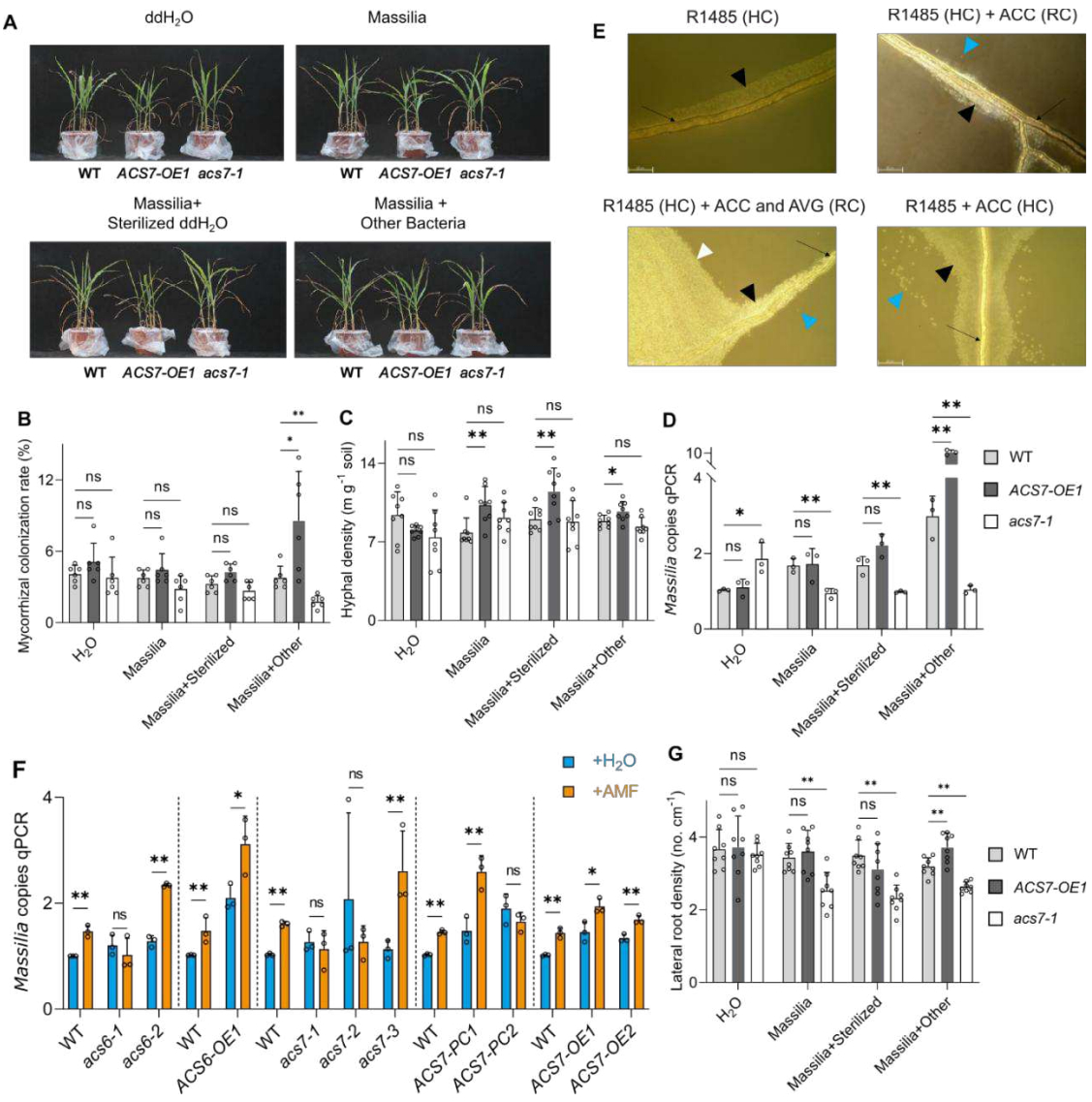


Figure 5. Ethylene mediates AM fungal cooperation with *Massilia* to enhance maize growth and phosphorus acquisition. (A) Growth responses of wild-type maize (B104), the ethylene biosynthesis mutant *acs7-1*, and overexpression line (ACS7-OE1) upon inoculation with either individual *Massilia* isolates or *Massilia*-based synthetic communities. **(B)** Mycorrhizal colonization rates are not significantly affected by genotype or *Massilia* treatment, indicating that ethylene does not alter AM fungal entry. n = 6 biologically independent replicates. **(C–D)** Ethylene biosynthesis is positively correlated with AM fungal hyphal length density (**C**) and *Massilia* enrichment in the rhizosphere (**D**) across treatments. n = 8 biologically independent replicates. **(E)** Supplementation of ACC (ethylene precursor) in the hyphal compartment enhances *Massilia* colonization along AM fungal hyphae, supporting ethylene-mediated hyphosphere recruitment. **(F)** AM fungal inoculation partially restores *Massilia* enrichment in ACS7 overexpression lines. n = 3 biologically independent replicates. Pairwise comparisons between treatments (+H_2O and +AMF) were performed within each genotype using two-sided Student's *t*-tests. Data are presented as mean ± s.e.m.; dots represent independent biological replicates. ns, not significant; *P < 0.05;

804 $^{**}P < 0.01$. **(G)** Ethylene biosynthesis is required for *Massilia*-induced lateral root development, as this
805 response is impaired in *acs7-1* and enhanced in ACS7-OE1. n = 8 biologically independent replicates. For
806 B-D and G, pairwise comparisons among genotypes (WT, ACS7-OE1 and *acs7-1*) were performed within
807 each treatment using two-sided Student's *t*-tests. Data are presented as mean ± SD; dots represent
808 independent biological replicates. ns, not significant; $^{*}P < 0.05$; $^{**}P < 0.01$.

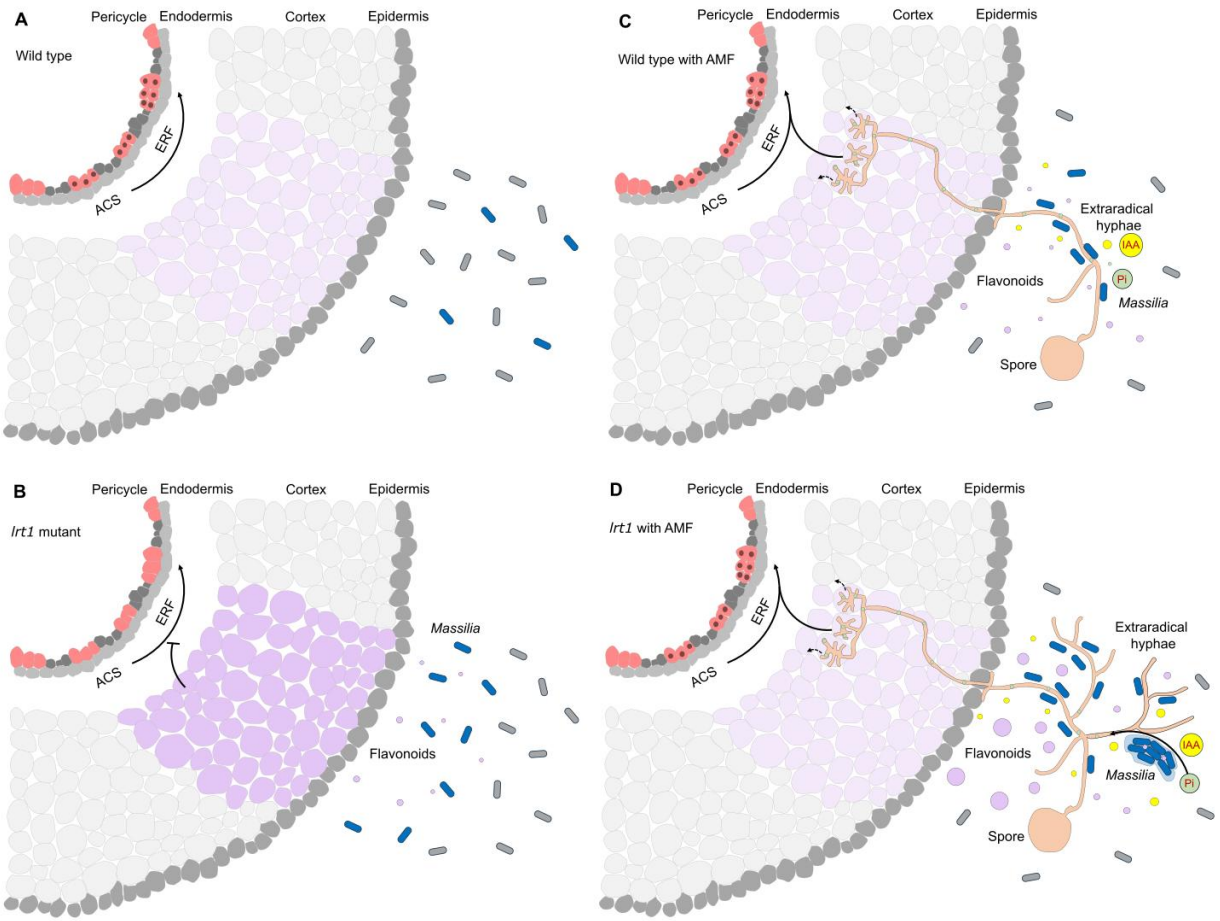


Figure 6. Working model linking ethylene signaling, flavonoid-associated metabolism, and AM fungus–related root responses under low-phosphate conditions. This model summarizes how ethylene biosynthesis and ERF-associated transcriptional activity are linked to lateral root development in maize, and how these processes are associated with arbuscular mycorrhizal (AM) fungal colonization. AM fungal presence is accompanied by changes in flavonoid-related metabolism and by the association of bacteria such as *Massilia* in the root-associated environment. Flavonoids are depicted as context-dependent chemical factors that may influence fungal and bacterial interactions, while ERF activity is associated with pericycle cell differentiation and lateral root formation (black dots). Together, these components represent interconnected processes contributing to root system adaptation under low-phosphate conditions, although several mechanistic links remain to be resolved. **(A)** In wild-type plants, the ZmACS–ZmERF signaling pathway regulates normal lateral root initiation, which occurs largely independently of rhizosphere bacterial microbiota. **(B)** In *lrt1* mutants, overaccumulation of flavonoids in the root cortex suppresses ERF gene expression, thereby inhibiting lateral root initiation. Although *Massilia* can still be partially recruited via flavonoid exudation, this is insufficient to restore normal root development. **(C)** In wild-type plants inoculated with AM fungi, extraradical hyphae associated with *Massilia*, promoting localized phosphorus solubilization and enhancing lateral root formation, providing an additional layer of symbiotic benefit. **(D)** In *lrt1* mutants colonized by AM fungi, cortical flavonoids are potentially redirected to the rhizosphere, where they enhance extraradical hyphal branching, promote *Massilia* enrichment, and facilitate biofilm formation on the hyphae. These interkingdom interactions stimulate auxin production, thereby partially restoring lateral root development despite disrupted host signaling.

References

Bailey, T.L., Boden, M., Buske, F.A., Frith, M., Grant, C.E., Clementi, L., Ren, J., Li, W.W., and Noble, W.S. 2009. MEME SUITE: tools for motif discovery and searching. Nucleic Acids Research 37, W202-W208.

Benjamini, Y., and Hochberg, Y. 1995. Controlling the false discovery rate: a practical and powerful approach to multiple testing. Journal of the Royal statistical society: series B (Methodological) 57, 289–300.

Bouwmeester, H., Dong, L., Wippel, K., Hofland, T., and Smilde, A. 2025. The chemical interaction between plants and the rhizosphere microbiome. Trends in Plant Science 30, 1002-1019.

Brundrett, M.M.L., and Peterson, L. 1994. Practical methods in mycorrhiza research. Mycologue Publication, University of Guelph, Canada.

Buee, M., Rossignol, M., Jauneau, A., Ranjeva, R., and Bécard, G. 2000. The pre-symbiotic growth of arbuscular mycorrhizal fungi is induced by a branching factor partially purified from plant root exudates. Molecular Plant-Microbe Interactions 13, 693-698.

Cai, X.T., Xu, P., Zhao, P.X., Liu, R., Yu, L.H., and Xiang, C.B. 2014. Arabidopsis ERF109 mediates cross-talk between jasmonic acid and auxin biosynthesis during lateral root formation. Nature Communications 5, 5833.

Chiu, C.H., Choi, J., and Paszkowski, U. 2018. Independent signalling cues underpin arbuscular mycorrhizal symbiosis and large lateral root induction in rice. New Phytologist 217, 552-557.

Chiu, C.H., Roszak, P., Orvošová, M., and Paszkowski, U. 2022. Arbuscular mycorrhizal fungi induce lateral root development in angiosperms via a conserved set of MAMP receptors. Current Biology 32, 4428-4437.

Cook, N.M., Gobbato, G., Jacott, C.N., Marchal, C., Hsieh, C.Y., Lam, A.H.C., Simmonds, J., Del Cerro, P., Gomez, P.N., Rodney, C. and Cruz-Mireles, N. 2025. Autoactive CNGC15 enhances root endosymbiosis in legume and wheat. Nature 638, 752-759.

Cranenbrouck, S., Voets, L., Bivort, C., Renard, L., Strullu, D.-G., andDeclerck, S. (2005). Methodologies for in vitro cultivation of arbuscular mycorrhizal fungi with root organs. In Vitro Culture of Mycorrhizas, 341-375.

Das, D., Varshney, K., Ogawa, S., Torabi, S., Hüttl, R., Nelson, D.C., and Gutjahr, C. 2025. Ethylene promotes SMAX1 accumulation to inhibit arbuscular mycorrhiza symbiosis. Nature Communications 16, 2025.

Della Vedova, C.B., Lorbiecke, R., Kirsch, H., Schulte, M.B., Scheets, K., Borchert, L.M., Scheffler, B.E., Wienand, U., Cone, K.C., and Birchler, J.A. 2005. The dominant inhibitory chalcone synthase allele C2-Idf (inhibitor diffuse) from Zea mays (L.) acts via an endogenous RNA silencing mechanism. Genetics 170, 1989-2002.

863 Desiro, A., Salvioli, A., Ngonkeu, E.L., Mondo, S.J., Epis, S., Faccio, A., Kaech, A., Pawlowska, T.E., and
864 Bonfante, P. 2014. Detection of a novel intracellular microbiome hosted in arbuscular mycorrhizal fungi. The
865 ISME Journal 8, 257-270.

866 Du, Z., Zhou, X., Ling, Y., Zhang, Z., and Su, Z. 2010. agriGO: a GO analysis toolkit for the agricultural
867 community. Nucleic Acids Research 38, W64-W70.

868 Duan, S., Feng, G., Limpens, E., Bonfante, P., Xie, X., and Zhang, L. 2024. Cross-kingdom nutrient
869 exchange in the plant–arbuscular mycorrhizal fungus–bacterium continuum. Nature Reviews Microbiology
870 22, 773-790.

871 Dubrovsky, J.G., Soukup, A., Napsucialy-Mendivil, S., Jeknić, Z., and Ivanchenko, M.G. 2009. The lateral
872 root initiation index: an integrative measure of primordium formation. Annals of Botany 103, 807-817.

873 Dunn, W.B., Broadhurst, D., Begley, P., Zelena, E., Francis-McIntyre, S., Anderson, N., and Nicholls, A.W.
874 2011. Procedures for large-scale metabolic profiling of serum and plasma using gas chromatography and
875 liquid chromatography coupled to mass spectrometry. Nature Protocols 6, 1060-1083.

876 Geisler-Lee, J., Caldwell, C., and Gallie, D.R. 2010. Expression of the ethylene biosynthetic machinery in
877 maize roots is regulated in response to hypoxia. Journal of Experimental Botany 61, 857-871.

878 Genre, A., Lanfranco, L., Perotto, S., and Bonfante, P. 2020. Unique and common traits in mycorrhizal
879 symbioses. Nature Reviews Microbiology, 1-12.

880 Gonin, M., Salas-González, I., Gopaulchan, D., Frene, J.P., Roden, S., Van de Poel, B., Salt, D.E., and
881 Castrillo, G. 2023. Plant microbiota controls an alternative root branching regulatory mechanism in plants.
882 Proceedings of the National Academy of Sciences 120, p.e2301054120.

883 Gutjahr, C., and Parniske, M. 2013. Cell and developmental biology of arbuscular mycorrhiza symbiosis.
884 Annual Review of Cell and Developmental Biology 29, 593-617.

885 Hassan, S., and Mathesius, U. 2012. The role of flavonoids in root–rhizosphere signalling: opportunities
886 and challenges for improving plant–microbe interactions. Journal of Experimental Botany 63, 3429-3444.

887 He, J., Van Dingenen, J., Goormachtig, S., Calonne-Salmon, M., and Declerck, S. 2025. Legume-specific
888 recruitment of rhizobia by hyphae of arbuscular mycorrhizal fungi. The ISME Journal 19, wraf100.

889 He, X., Wang, D., Jiang, Y., Li, M., Delgado-Baquerizo, M., McLaughlin, C., Marcon, C., Guo, L., Baer, M.,
890 Moya, Y.A.T., von Wirén, N., Deichmann, M., Schaaf, G., Piepho, H-P., Yang, Z., Yang, J., Yim, B., Smalla,
891 K., Goormachtig, S., de Vries, F., Hüging, H., Sawers, R.J.H, Reif, J.C., Hochholdinger, F., Chen, X., and
892 Yu, P. 2024. Heritable microbiome variation is correlated with source environment in locally adapted maize
893 varieties. Nature Plants 10: 598–617.

Hochholdinger, F., and Feix, G. 1998. Early post-embryonic root formation is specifically affected in the maize mutant lrt1. The Plant Journal 16, 247– 255.

Hochholdinger, F., Yu, P., and Marcon, C. 2018. Genetic control of root system development in maize. Trends in Plant Science 23, 79-88.

Jin, Z., Jiang, F., Wang, L., Declerck, S., Feng, G., and Zhang, L. 2024. Arbuscular mycorrhizal fungi and Streptomyces: brothers in arms to shape the structure and function of the hyphosphere microbiome in the early stage of interaction. Microbiome 12, 83.

Lanfranco, L., Fiorilli, V., and Gutjahr, C. 2018. Partner communication and role of nutrients in the arbuscular mycorrhizal symbiosis. New Phytologist 220, 1031-1046.

Lee, M., Sharopova, N., Beavis, W.D., Grant, D., Katt, M., Blair, D., and Hallauer, A. 2002. Expanding the genetic map of maize with the intermated B73× Mo17 (IBM) population. Plant Molecular Biology 48, 453-461.

Li, H., Wang, L., Liu, M., Dong, Z., Li, Q., Fei, S., Xiang, H., Liu, B., and Jin, W. 2020. Maize plant architecture is regulated by the ethylene biosynthetic gene ZmACS7. Plant Physiology 183, 1184-1199.

Li, X., Zhao, R., Li, D., Wang, G., Bei, S., Ju, X., An, R., Li, L., Kuyper, T.W., Christie, P., and Bender, F.S. 2023. Mycorrhiza-mediated recruitment of complete denitrifying Pseudomonas reduces N_2O emissions from soil. Microbiome 11, 45.

Lidoy, J., Berrio, E., García, M., España-Luque, L., Pozo, M.J., and López-Ráez, J.A. 2023. Flavonoids promote Rhizophagus irregularis spore germination and tomato root colonization: A target for sustainable agriculture. Frontiers in Plant Science 13, 1094194.

Lim, J., Helariutta, Y., Specht, C.D., Jung, J., Sims, L., Bruce, W.B., Diehn, S., and Benfey, P.N. 2000. Molecular analysis of the SCARECROW gene in maize reveals a common basis for radial patterning in diverse meristems. Plant Cell 12, 1307–1318

MacLean, A.M., Bravo, A., and Harrison, M.J. 2017. Plant signaling and metabolic pathways enabling arbuscular mycorrhizal symbiosis. The Plant Cell 29, 2319-2335.

Malamy, J.E., and Benfey, P.N. 1997. Organization and cell differentiation in lateral roots of Arabidopsis thaliana. Development 124, 33–44.

Mathelier, A., Zhao, X., Zhang, A.W., Parcy, F., Worsley-Hunt, R., Arenillas, D.J., Buchman, S., Chen, C., Chou, A., Ienasescu, H., Lim, J., Shyr, A., Tan, G., Zhou, M., Lenhard, B., Sandelin, A., and Wasserman, W.W. 2014. JASPAR 2014: an extensively expanded and updated open-access database of transcription factor binding profiles. Nucleic Acids Research 42, D142-D147.

925 Paszkowski, U., and Boller, T. 2002. The growth defect oflrt1,a maize mutant lacking lateral roots, can be
926 complemented by symbiotic fungi or high phosphate nutrition. Planta 214, 584–590.

927 Paszkowski, U., Jakovleva, L., and Boller, T. 2006. Maize mutants affected at distinct stages of the
928 arbuscular mycorrhizal symbiosis. The Plant Journal 47, 165–173.

929 Phillips, J.M., and Hayman, D.S. 1970. Improved procedures for clearing roots and staining parasitic and
930 vesicular-arbuscular mycorrhizal fungi for rapid assessment of infection. Transactions of the British
931 Mycological Society 55, 158-161.

932 Qi, W., Zhu, T., Tian, Z., Li, C., Zhang, W., and Song, R. 2016. High-efficiency CRISPR/Cas9 multiplex gene
933 editing using the glycine tRNA-processing system-based strategy in maize. BMC Biotechnology 16, 58.

934 Scervino, J.M., Ponce, M.A., Erra-Bassells, R., Bompadre, J., Vierheilig, H., Ocampo, J.A., and Godeas, A.
935 2007. The effect of flavones and flavonols on colonization of tomato plants by arbuscular mycorrhizal fungi
936 of the genera Gigaspora and Glomus. Canadian Journal of Microbiology 53, 702-709.

937 Scervino, J.M., Ponce, M.A., Erra-Bassells, R., Bompadre, M.J., Vierheilig, H., Ocampo, J.A., and Godeas,
938 A. 2006. Glycosidation of apigenin results in a loss of its activity on different growth parameters of
939 arbuscular mycorrhizal fungi from the genus Glomus and Gigaspora. Soil Biology and Biochemistry 38,
940 2919-2922.

941 Scervino, J.M., Ponce, M.A., Erra-Bassells, R., Vierheilig, H., Ocampo, J.A., and Godeas, A. 2005.
942 Flavonoids exhibit fungal species and genus specific effects on the presymbiotic growth of Gigaspora and
943 Glomus. Mycological Research 109, 789-794.

944 Schlicht, M., Ludwig-Müller, J., Burbach, C., Volkmann, D., and Baluska, F. 2013. Indole-3-butyric acid
945 induces lateral root formation via peroxisome-derived indole-3-acetic acid and nitric oxide. New
946 Phytologist 200, 473-482.

947 Smyth, G.K. 2004. Linear models and empirical Bayes methods for assessing differential expression in
948 microarray experiments. Statistical Applications in Genetics and Molecular Biology 1, 3.

949 Soon, Y.K., and Kalra, Y.P. 1995. A comparison of plant tissue digestion methods for nitrogen and
950 phosphorus analyses. Canadian Journal of Soil Science 75, 243-254.

951 St-Arnaud, M., Hamel, C., Vimard, B., Caron, M. & Fortin, J. A. (1996). Enhanced hyphal growth and spore
952 production of the arbuscular mycorrhizal fungus *Glomus intraradices* in an in vitro system in absence of
953 host roots. Mycological Research 100, 328–332.

954 Stringlis, I.A., Yu, K.E., Feussner, K., de Jonge, R., Van Bentum, S., Van Verk, M.C., Berendsen, R.L.,
955 Bakker, P.A., Feussner, I., and Pieterse, C.M. 2018. MYB72-dependent coumarin exudation shapes root
956 microbiome assembly to promote plant health. Proceedings of the National Academy of Sciences 115,
957 5213-5222.

Sun, N., Wang, L., and Feng, G. 2025. Host-dependent roles of hyphosphere keystone Massilia in organic phosphorus mineralization and arbuscular mycorrhizal fungal growth. Journal of Experimental Botany, eraf339.

Szklarczyk, D., Franceschini, A., Wyder, S., Forslund, K., Heller, D., Huerta-Cepas, J., Simonovic, M., Roth, A., Santos, A., Tsafou, K.P., Kuhn, M., Bork, P., Jensen, L.J., and von Mering, C. 2015. STRING v10: protein-protein interaction networks, integrated over the tree of life. Nucleic Acids Research 43, D447–D452.

Tian, B., Pei, Y., Huang, W., Ding, J., and Siemann, E. 2021. Increasing flavonoid concentrations in root exudates enhance associations between arbuscular mycorrhizal fungi and an invasive plant. The ISME Journal 15, 1919-1930.

Trouvelot, A., Kough, J., and Gianinazzi-Pearson, V. 1986. Mesure du taux de mycorhization VA d'un système radiculaire. Recherche de méthodes d'estimation ayant une signification fonctionnelle. In:Gianinazzi-Pearson V, Gianinazzi S (eds) Physiological and Genetical Aspects of Mycorrhizae. INRA Press, Paris.

Van Norman, J.M., Xuan, W., Beeckman, T., and Benfey, P.N. 2013. To branch or not to branch: the role of pre-patterning in lateral root formation. Development 140, 4301-4310.

Wang, L., Chen, M., Lam, P.Y., Dini-Andreote, F., Dai, L., and Wei, Z. 2022. Multifaceted roles of flavonoids mediating plant-microbe interactions. Microbiome, 10, 233.

Wang, L., Zhang, L., George, T.S., and Feng, G. 2025. Hyphosphere core taxa link plant-arbuscular mycorrhizal fungi combinations to soil organic phosphorus mineralization. Soil Biology and Biochemistry 201, 109647.

Wen, B., Zhou, R., Feng, Q., Wang, Q., Wang, J., and Liu, S. 2014. IQuant: an automated pipeline for quantitative proteomics based upon isobaric tags. Proteomics 14, 2280-2285.

Wu, J., Liu, S., Zhang, H., Chen, S., Si, J., Liu, L., Wang, Y., Tan, S., Du, Y., Jin, Z., Xie, J., and Zhang, D. 2025. Flavones enrich rhizosphere Pseudomonas to enhance nitrogen utilization and secondary root growth in Populus. Nature Communications 16, 1461.

Xue, L., Almario, J., Fabiańska, I., Saridis, G., and Bucher, M. 2019. Dysfunction in the arbuscular mycorrhizal symbiosis has consistent but small effects on the establishment of the fungal microbiota in *Lotus japonicus*. New Phytologist 224, 409-420.

Yeung, K.Y., Fraley, C., Murua, A., Raftery, A.E., and Ruzzo, W.L. 2001. Model-based clustering and data transformations for gene expression data. Bioinformatics 17, 977–987.

Yu, P., Baldauf, J.A., Lithio, A., Marcon, C., Nettleton, D., Li, C., and Hochholdinger, F. 2016. Root type specific reprogramming of maize pericycle transcriptomes by local high nitrate results in disparate lateral root branching patterns. Plant Physiology 170, 1783–1798.

Yu, P., Eggert, K., von Wirén, N., Li, C., and Hochholdinger, F. 2015. Cell type-specific gene expression analyses by RNA sequencing reveal local high nitrate-triggered lateral root initiation in shoot-borne roots of maize by modulating auxin-related cell cycle regulation. Plant Physiology 169, 690-704.

Yu, P., Gutjahr, C., Li, C., and Hochholdinger, F. 2016. Genetic control of lateral root formation in cereals. Trends in Plant Science 21, 951-961.

Yu, P., He, X., Baer, M., Beirinckx, S., Tian, T., Moya, Y.A.T., Zhang, Y., Deichmann, M., Frey, F.P., Bresgen, V., Li, C., Razavi, B.S., Schaaf, G., von Wirén, N., Su, Z., Bucher, M., Tsuda, K., Goormachtig, S., Chen, X., and Hochholdinger, F. 2021. Plant flavones enrich rhizosphere Oxalobacteraceae to improve maize performance under nitrogen deprivation. Nature Plants 7, 481–499.

Zhang, C., van der Heijden, M.G., Dodds, B.K., Nguyen, T.B., Spooren, J., Valzano-Held, A., Cosme, M., and Berendsen, R.L. 2024. A tripartite bacterial-fungal-plant symbiosis in the mycorrhiza-shaped microbiome drives plant growth and mycorrhization. Microbiome 12, 13.

Zhang, X., Jin, X., Li, J., Dini-Andreote, F., Li, H., u Rahman, M.K., Du, M., Wu, F., Wei, Z., Zhou, X., van der Heijden, M., and Rillig, M.C. 2025. Common mycorrhizal networks facilitate plant disease resistance by altering rhizosphere microbiome assembly. Cell Host & Microbe 33, 1765-1778.

Zhao, J., Chen, Y., Tao, Q., Schreiber, L., Suresh, K., Frei M Alam, M.S., Li, B., Zhou, Y., Baer, M., Hochholdinger, F., Wang, C., and Yu, P. 2024. Enhanced CO_2 coordinates the spatial recruitment of diazotrophs in rice via root development. Plant Cell and Environment, 1–16.

Zhu, J., Song, N., Sun, S., Yang, W., Zhao, H., Song, W., and Lai, J. 2016. Efficiency and inheritance of targeted mutagenesis in maize using CRISPR-Cas9. Journal of Genetics and Genomics 43, 25-36.

Supplementary Files

This is a list of supplementary files associated with this preprint. Click to download.

- Supplementaryfiguresandtables.pdf